




Article

A Forty-Year Karstic Critical Zone Survey (Baget Catchment, Pyrenees-France): Lithologic and Hydroclimatic Controls on Seasonal and Inter-Annual Variations of Stream Water Chemical Composition, $p\text{CO}_2$, and Carbonate Equilibrium

Francesco Ulloa-Cedamano^{1,2,3,*}, Jean-Luc Probst^{1,2,3}, Stephane Binet^{1,4},
Thierry Camboulive^{1,2,3}, Virginie Payre-Suc^{1,2,3}, Corinne Pautot^{1,2,3}, Michel Bakalowicz⁵,
Sandra Beranger⁶ and Anne Probst^{1,2,3,*}

- ¹ Laboratoire écologie fonctionnelle et environnement, Université de Toulouse, CNRS, UPS, INPT, Campus ENSAT, 31326 Castanet Tolosan, France; jean-luc.probst@toulouse-inp.fr (J.-L.P.); stephane.binet@univ-orleans.fr (S.B.); thierry.camboulive@univ-tlse3.fr (T.C.); virginie.payre@ensat.fr (V.P.S.); corinne.pautot@toulouse-inp.fr (C.P.)
 - ² Long-Term Socio-Ecological Research, Zone Atelier Pyrénées-Garonne, CNRS, Université de Toulouse, Campus ENSAT, 31326 Castanet Tolosan, France
 - ³ Long-Term Ecosystem Research, Bassin versant du Baget, SNO Karst, IR OZCAR, CNRS, Université de Toulouse, Campus ENSAT, 31326 Castanet Tolosan, France
 - ⁴ Institut des Sciences de la Terre d'Orléans, Université d'Orléans, CNRS, BRGM, 45100 Orléans, France
 - ⁵ HydroSciences Montpellier, Université de Montpellier, CNRS, 34095 Montpellier, France; michel.bakalowicz@gmail.com
 - ⁶ Bureau de Recherches Géologiques et Minières—Délégation Régionale Occitanie-Site de Toulouse, 31520 Ramonville-Saint-Agne, France; s.beranger@brgm.fr
- * Correspondence: francesco.ulloacedamano@toulouse-inp.fr (F.U.-C.); anne.probst@ensat.fr (A.P.)

Received: 26 March 2020; Accepted: 20 April 2020; Published: 25 April 2020



Abstract: The long-term trends and seasonal patterns of stream water chemical composition in a small remote forested karst catchment, were investigated from 1978 to 2018. Calcium, magnesium, and bicarbonates, the dominant ions, increased over the period together with temperature, while sulfates decreased. Carbonate and sulfate mineral dissolution was the main source of these elements. These trends and the seasonal opposite patterns of discharge vs. temperature, calcite saturation index vs. $p\text{CO}_2$ and bicarbonate vs. sulfates, suggested the influence of discharge, of reduced long-range atmospheric pollution, and of increasing air temperature on biological activity and carbonate dissolution. Furthermore, the hydrological regime controlled the seasonal stream water chemical composition and fluxes by: (i) a dilution during the high discharge period, (ii) a change in the contribution rate of the waters draining different lithological areas in the catchment, e.g., the increased sulfates to bicarbonates ratio during summer low flows, with a maximum alkalinity decrease of 24%, and (iii) a “piston” and a “flushing” effects of dissolved elements stored in soils and epikarst with the first autumn heavy rains. Long-term stream water hydrochemical surveys of karst system have proved to be powerful indicators of biogeochemical processes, water sources and pathways under variable natural and anthropogenic environmental pressure conditions.

Keywords: long-term monitoring; hydrochemical trends; carbonate dissolution; mineral weathering; seasonal patterns; global warming; mountainous catchment

1. Introduction

The increasing trend of CO₂ has a feedback effect on climate change and noticeably on the frequency of extreme hydro-climatic events [1–3]. The atmospheric CO₂ sink and the transfer of dissolved inorganic carbon (DIC) from the atmosphere to the critical zone and to the oceans, via the rivers is greatly controlled by carbonate dissolution [4,5]. Although carbonates constitute between 10–15% of the continental surfaces [6–9], their chemical weathering has an important role: (i) in the annual production of dissolved elements exported (between 45% and 60%) annually by rivers to the oceans [5,10] and (ii) in the consumption of atmospheric/soil CO₂ (0.38 Gt-yr⁻¹) at the global scale [7]. Even though carbonate dissolution is the main part of the karstification process, it is not considered on a global scale as a carbon sink over geological timescales [11] because carbonate precipitation in the oceans (source of CO₂) compensates carbonate dissolution on the continents (sink of CO₂). However, its role on regulating global atmospheric CO₂ becomes relevant over short timescales. This is due to the quick kinetic dissolution [12] getting to the control of DIC concentrations in almost all carbonated catchment areas [13–17].

In addition, karst aquifers provide almost 25% of the water used for drinking water supply [8] and about half of the world's karst area lies between latitudes 20° and 40° north [7]. Furthermore, mountainous areas in southern Europe appear to be particularly vulnerable and sensitive to climate change [18–22] and also to land cover changes [23,24]. This is the case of the Pyrenees Mountains (South of France), which are expected to be severely affected by environmental perturbations during the 21st century, mainly with the decrease in water availability [25,26].

The karst system is mainly recharged by rainwater, where water seepage is enabled by the fractured and karstic nature of the calcareous rock [27]. The karst system includes both the infiltration zone (including epikarst) and the saturated zone, and by extension, the hydrological system that flows in the fractures and in the conduits formed mainly by the dissolution of carbonate rock [28]. Epikarst is the quasi-permanent shallow and discontinuous saturated layer, where the infiltrated water dissolves the carbonate mineral and changes the geochemical features of the rock [29]. Indeed, the main agent of the dissolution of carbonates is the biogenic CO₂, supplied by the organic matter mineralization and stored in the soil, a few meters above the epikarst [30]. However, the CO₂–H₂O–Ca_(1-x)Mg_(x)CO₃ system is sensitive to environmental changes due to karstic characteristics such as high transmissivity (lower residence time), high dissolution kinetics, and low filtering role of the infiltration zone [31].

Among the parameters that play a role in the dissolution of carbonates, we can highlight hydrology [29,32], climate [17,33], land-use/vegetation [34,35], lithology [7,36,37], and human activities [38,39].

Several studies have shown the strong control that runoff has over carbonate dissolution flow [7,40]. Moreover, during the high flow period, the huge and rapid water flow through the karstic network could reduce the dissolution due to less water-rock interaction [41] but on the opposite, enhance the dissolution by renewal of the solutions in contact with the mineral [42]. Then, it may also explain a gradual increase in element concentrations as runoff increases.

Temperature is another parameter which strongly influences carbonate dissolution. Thermodynamically, an increase in temperature leads to a decrease in carbonate solubility [43–45]. However, increasing temperatures also enhance biological activity and decomposition of soil organic matter, causing an increasing pCO₂, carbonic acid, and organic acid contents in the critical zone, particularly in epikarsts and caves, accelerating carbonate dissolution [34,46–48]. In addition, based on a global database of pure carbonate lithologies, Probst [49], Amiotte-Suchet et al. [7], and Gaillardet et al. [50] evidenced a control of temperature over carbonate weathering intensity, with a Ca²⁺ + Mg²⁺ concentration peak in river water under temperate conditions.

The CO₂ mainly originates from atmospheric and soil sources. Vegetation plays a key role in sequestering and storing atmospheric CO₂ to be transformed into organic matter [51]. Subsequently, the decomposition of organic matter and root respiration lead to the production of CO₂ in soils [52]. Between these two CO₂ sources, the direct input of atmospheric CO₂ to the soils is usually low due to

high pressure of soil CO₂ and low pH values (lower than 5.6) of rainwater [53]. The dissolution of CO₂, mainly resulting from the oxidation of organic matter, is illustrated by the following chemical reactions:



Furthermore, in recent years, increases of pCO₂ in soils and caves [33,54], total dissolved solids (TDS) and alkalinity in rivers have been observed [55–57]. In the meantime, the reduction of annual streamflows, particularly in Mediterranean rivers was evidenced [58–60]. These changes suggest the intervention of external driving factors such as climate change [61–63] and/or land use change [24,38,64,65].

Carbonate dissolution can also be carried out by chemical agents other than carbonic acid. Anthropogenic disturbances such as agricultural practices using N-fertilizers [66–68], atmospheric deposition from long-distance sources of air pollution [69–72] and acid mine drainage [73,74], are potential sources of sulfuric and nitric acids that can add to or substitute carbonic acid in carbonate dissolution process. Likewise, there are also natural sources of sulfuric acid from volcanoes and hot springs as well as sulfur minerals in soils and sediments [75,76]. Additionally, by enhancing the capture of dry deposition, coniferous forests can contribute to the increase in sulfuric acid inputs to soils by atmospheric deposition (dry and wet deposition), particularly from throughfalls [77,78] at the catchment scale. Unlike carbonate dissolution by carbonic acid that generates two moles of bicarbonates consuming one mole of CO₂, sulfuric and nitric acids only release one mole of bicarbonates, which could escape from the water in the form of gas (CO₂ gas), or could enter seepage water and dissolves carbonate again (aqueous CO₂) [39].

In this context, the Baget catchment in the Pyrenees Mountains, was selected as a research area to analyze the fluctuations of physico-chemical composition of stream waters over a 40-years period. This catchment has been already extensively studied using time series data for a hydrological perspective [79–81] and for some chemical parameters until 2005 [82,83]. However, this is the first time that all the hydrogeochemical data available between 1978 and 2018 were investigated and the pCO₂ in stream water was reconstituted at both interannual and seasonal scales. Then, long-term trends as well as interannual seasonal variations for all the physico-chemical parameters allow to better understand the karst biogeochemical functioning.

The objectives were: (i) to investigate the variation of discharge, temperature, CO₂, SI_c (Calcite Saturation Index), and major element concentrations in the river water using long-term surveys at various time scales (instantaneous, monthly, and annual values); (ii) to depict the impact of global changes on carbonate dissolution and hydrochemistry of stream waters; (iii) to elucidate the key factors controlling carbonate dissolution (such as temperature, discharge, and vegetation), and the respective contributions of water sources, particularly from karst and epikarst; and iv) to understand the dynamics of CO₂, carbonate dissolution, and stream water chemistry.

According to described uplines, several hypotheses were set up to explain the observed trends. At the year scale, the discharge would cause an increase in carbonate dissolution, but with a dilution effect during the highest flow conditions. The increase in air temperature should finally enhance indirectly carbonate dissolution due to the rise in organic matter mineralization and production of carbonic and organic acids, even if carbonate solubility would decrease with temperature increase [82]. Therefore, an increase in global air temperature and change in land use, i.e., from crops or grasslands to forest, should increase carbonate dissolution on the long-term. However, other external anthropic pressures might add other drivers to the karstic system and change the dynamic of carbonate dissolution.

2. Materials and Methods

2.1. Site Description

The small Baget catchment (BC, 13.25 km²; 42°57'42" N 0°58'30" E; Figure 1) is located in the lower part of the Pyrenees Mountains, in the Ariège department, in the Southwest of France. Its altitude ranges from 498 to 1417 m.s.l., with a water flow orientation from West to East [84]. Slopes are very steep, particularly in the middle part of the basin, where they reach 60% [79].

BC drains a karst area, mainly in the calcareous formation of the Jurassic and Lower Cretaceous, relatively homogeneous at the outcrop and with a mineralogical composition usually greater than 98% of calcite. However, they are associated with pyrite, which is sometimes abundant in the area of contact with the impermeable formation of black flysch (Figure 1b) [83]. Some schists (with small pyrite impurities), minor gypsum rocks and dolomitic rocks were also observed in the BC [85].

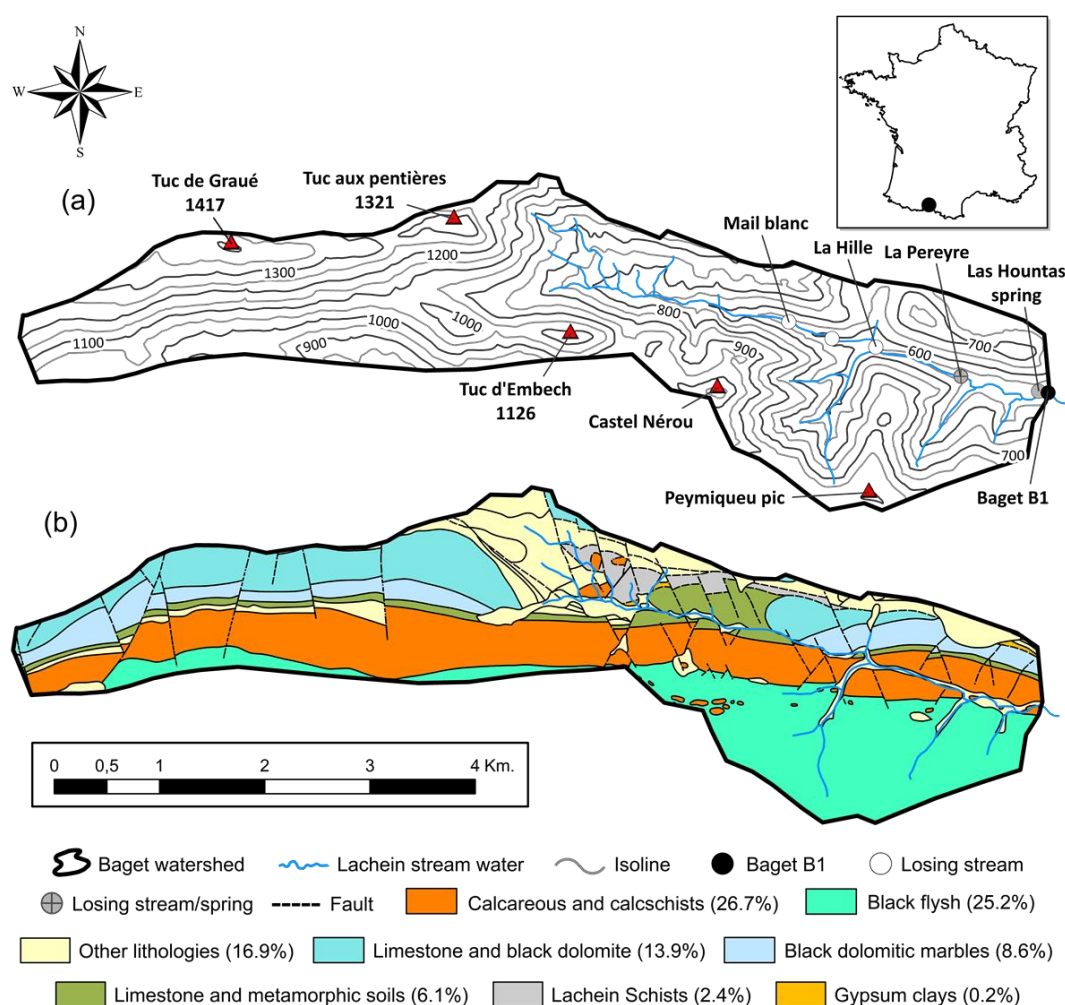


Figure 1. Location of the Baget karstic catchment with: (a) altitude isolines (modified from Labat et al. [80]) and (b) lithology based on main formations (1/50,000) modified from BRGM [86], this study).

The catchment is essentially forested. The land cover is dominated by fir-beech forests and it is particularly dense on the north-facing slope, whereas, grassland occupies partly the upper part and the lower part close to the outlet of the south-facing slope. Although there is an extensive vegetation, the soils are generally very thin. The limestones are covered by discontinuous brown soils, sometimes with rendzina soils, generally occupying the limestone pavement slits. Podzols are developed on detrital formations. The grasslands are located on podzolic soils well exposed to the south near to the

Lachein stream water and also, in the bottom of the valley, downstream, on the alluvium [83]. BC is weakly exposed to local anthropogenic pollution with only few remaining mountain stockbreeding on the upper part of the south facing slope.

BC is under the influence of the Atlantic oceanic climate characterized by a clear mountain tendency with an average annual air temperature of 12.3 °C, an average annual rainfall close to 1700 mm and an estimated annual evapotranspiration of 540 mm [79,87,88]. Those values are close to the daily average air temperature of 12.0 ± 6.3 °C and higher than the annual average rainfall of 975.5 mm, registered at the closest Meteo-France meteorological station of St. Girons (43°00'19" N 1°06'25" E, elevation 414 m), located 8.3 km downstream from the outlet of BC. The precipitation gradient between the two stations is of +138 mm/100 m, which is close to that reported for the Jura Mountains [34], but much greater than that mentioned by Joly [89] for the Pyrenees Mountains (>25 mm/100 m). Indeed, this gradient depends on factors such as wind direction, relief, distance to the ocean and latitude, highly variable in mountainous areas [90].

The runoff which drains calcareous lithology can be lost through seepage or in losses of the Lachein stream water (e.g., losses of "La Hille" and "La Peyrère", this last one performing as a spring during flood period, Figure 1a), thus feeding the Baget groundwater karstic network. Downstream of the Baget valley, the Lachein stream water (usually dried up in summer) connects with the main perennial spring of the Baget karst system called "Las Hountas" (Figure 1a) [79]. The high-water flow period (from November to April) displays a bimodal rainfall regime with usually a first peak in December and a second one in February [79]. Considering the mean altitude, the storage of water in the form of snow is low and snowmelt does not result in significant increases in discharge. The average annual discharge is $0.48 \text{ m}^3 \cdot \text{s}^{-1}$ with a specific discharge of $36 \text{ L} \cdot \text{s}^{-1} \cdot \text{km}^{-2}$ [79,91], as measured at the outlet station (Baget B1, Figure 1a).

This experimental catchment belongs to the French Karst Network (SNO Karst, Jourde et al., 2018) [92] and is one of the observatories of the French Research Infrastructure called OZCAR (Observatoire de la Zone Critique: Application et Recherche) [93], which is part of the European Research Infrastructure eLTER (Long Term Ecosystem Research in Europe) [94,95].

2.2. Sampling and Analytical Methods

The hydrochemical monitoring station is located at the outlet of the catchment (Baget B1, Figure 1a). The water level was measured continuously using a mechanical limnigraph (OTT 20 1/5) and a float-type water level sensor (OTT Thalimedes) [96]. Discharge is estimated from the rating curve calibrated for this gauging station [79]. For water quality purpose, we used, the samples collected weekly from 1978 to 2006 by the CNRS "Laboratoire Souterrain de Moulis" [82] and every six months from 2007 to 2014 by the Adour-Garonne Water Agency (accessible via the ADES database, BRGM) [96]. By 2014, water sampling and hydrochemical parameters analyses were performed by EcoLab (Laboratoire Ecologie fonctionnelle et Environnement in Toulouse), fortnightly and more frequently during flood events using an automatic sampler. It should be noted that in 1990, a long-term pumping test dried the Baget spring ("Las Hountas"), so no data was available for part of this year.

From 1978 to 2006, pH, total carbonate alkalinity (in $\text{mmol} \cdot \text{L}^{-1}$; $0.2 \text{ TAC} = \text{HCO}_3^-$) and total water hardness (in $\text{mmol} \cdot \text{L}^{-1}$; $0.1 \text{ TWH} = \text{Ca}^{2+} + \text{Mg}^{2+}$, $R^2 = 0.92$, $N = 541$) were measured using a titrimetric method. Major ions were analyzed by ion chromatography.

Since April 2014, pH, pressure (water level), conductivity, water temperature, turbidity, dissolved O_2 , N-NO_3^- , and Cl^- concentrations were registered at a high frequency (every 10 mn) in the mid-depth of the water column (at Baget B1) using a multiparameter probe (YSI 6920V2-01, YSI Incorporated, Yellow Springs, OH, USA) equipped with different sensors and an atmospheric pressure correction. Moreover, from 2017 to present-day, a portable multi-parameter (WTW probe, Xylem Analytics Germany Sales GmbH & Co., Weilheim, Germany) was used to measure physicochemical parameters of water in the field, including water temperature (WT), pH, and electrical conductivity (EC) at the time of sampling.

Samples were collected in polypropylene plastic bottles of 1 L, then filtered immediately back to field in the laboratory using a Millipore 0.22 µm cellulose nitrate membrane. Since 2014, the protocol for sample treatment in the laboratory is as follows: firstly, an aliquot of 125 mL was taken to measure cation concentrations. This sub-sample was acidified with 3 drops of 16N HNO₃ (to prevent complexation and precipitation) and stored until the analyze by inductively coupled plasma optical emission spectrometer (ICP-OES; Iris Intrepid II XLD, Thermo Electron, Thermo Fisher Scientific, Waltham, MA, USA); secondly, an aliquot of 2 mL was used to analyze major anion concentrations (SO₄²⁻, NO₃⁻, and Cl⁻) by ion chromatography (Dionex apparatus ICS 5000+, Thermo Fisher Scientific, Waltham, MA, USA); lastly, an aliquot of 20 mL was taken to measure alkalinity concentration using standard acid titration method with HCl 0.02N and a Metrohm titrant (716 DMS Titrino, Metrohm, Riverview, Florida, USA) within 12 h after sampling. DOC was analyzed on a Shimadzu TOC 5000 analyzer (Shimadzu Corporation, Kyoto, Japan) using the 680 °C combustion catalytic oxidation method and CO₂ detection using an infrared gas analyzer (NDIR). All samples were stored in darkness at 5 °C before analysis.

Concerning the quality assurance (QA) and the quality control (QC), the data set is too long to have a QA/QC procedure over the whole period from 1978 until 2018. Anyway, concerning the QA, the protocols for sampling, filtration, pre-treatment and storage of the stream water before analysis were carefully controlled during the whole period. Concerning the QC, all the methods of analysis are normalized following French (NF), European (EN), and international (ISO) standards. The accuracy of analyses was controlled using blanks and two Certified Reference Materials (ION-96.4 and ION SUPER 05) depending on the range of ion concentration. The detection limits for major ions range between 0.2 and 65 µmol·L⁻¹ according to the elements.

For each sample analysis, the Net Inorganic Charge Balance (NICB % = 100 × (TZ⁺ - TZ⁻)/(TZ⁺ + TZ⁻)) between the sum of cations (TZ⁺) and the sum of anions (TZ⁻) (considered both in meq·L⁻¹) was calculated and was inferior to 5% for almost all samples, indicating that there is a good equilibrium between cation and anion charges, and consequently that the contribution of organic anions to the anionic charge remain negligible. This is confirmed by the low DOC concentrations (0.82 ± 0.79 mg·L⁻¹, N = 39, from November 2016 to September 2018).

Furthermore, since several decades, the physico-chemical analysis laboratory of EcoLab participates each year to the ICP-Water Intercomparison with the Norwegian Institute for Water Research (NIVA), which follows a QA/QC procedure.

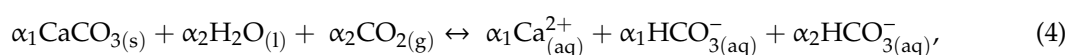
2.3. Data Treatment

2.3.1. pCO₂ and Calcite Saturation Index (SI_c)

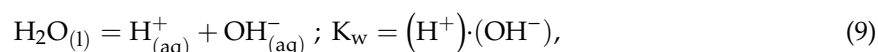
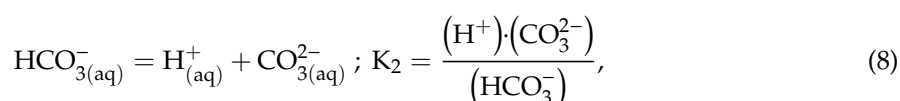
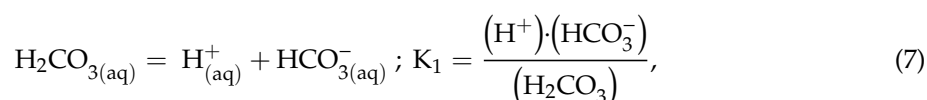
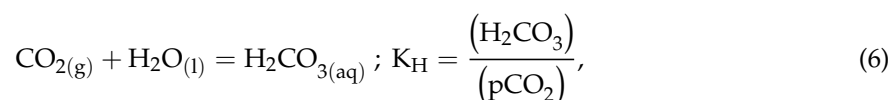
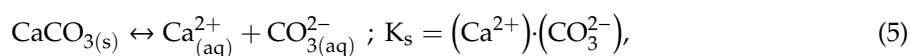
The partial pressure of carbon dioxide (pCO₂) and calcite saturation index (SI_c) were calculated using the mass equation. The calculations were computed with Phreeqc Interactive 3.4 software and the database "phreeqc.dat" [44], using the analyzed major element concentrations in stream water as well as the physicochemical parameters measured in the field during the water sampling.

In addition, stream water temperature was necessary to calculate pCO₂. The air temperature available for the full period and the water temperature available from 2014 to 2018 (N = 73) confirmed that the water temperature in stream varied very slightly during the year (from 9.5 to 11 °C). It could thus be estimated using the air temperature in centigrade degrees ($T_{\text{water}} = 0.03 T_{\text{air}} + 9.93$, R = 0.6, N = 59, *p*-value < 0.0001).

Due to the absence of concentration data for some major ions (SO₄²⁻; Cl⁻; NO₃⁻, Na⁺, and K⁺) during certain time slots, pCO₂ was also calculated manually, assuming the dissolution of pure calcite and using the following chemical reaction [97]:



The coefficients α_1 and α_2 had the same value but showed that, when the dissolution of carbonates by carbonic acid, one bicarbonate ion came from the mineral dissolution and the other one came from the consumption of atmospheric/soil CO_2 .



where the round parenthesis represents the activities of the respective species, and K , the equilibrium constants calculated using the temperature dependence of thermodynamic constants defined by Plummer and Busenberg [98].

Assuming that the dissolution of carbonates took place under open system conditions and in equilibrium with regard to calcite, the Ca^{2+} or pCO_2 could be estimated using the following equation:

$$(\text{Ca}^{2+}) = \left(\frac{K_1 K_H K_s}{4 K_2 \gamma_1^2 \gamma_2} \text{pCO}_2 \right)^{\frac{1}{3}}, \quad (10)$$

where γ_1 and γ_2 , the ion activity coefficients for single-charge and dual-charge species, respectively. These activity coefficients were calculated using the Davies equation [99] with the PhreeqC Interactive 3.4 software [44].

These pCO_2 values calculated using the PhreeqC Interactive 3.4 software and manually calculations for the periods 1994–2006 and 2016–2018 confirmed that both results are consistent ($R^2 = 1.00$).

Likewise, the calcite saturation indexes were calculated using the thermodynamic constant K_s (solubility product of calcite) at given water temperature, as given below by Clark and Fritz [97]:

$$\text{SIc} = \log((\text{Ca}^{2+}) \cdot (\text{CO}_3^{2-})) / K_s, \quad (11)$$

2.3.2. Statistics

All calculations were computed on a hydrological year basis (October–September). For simplicity, only the second year of each period will be indicated, for example the period from October 1978 to September 1979 will be shown as the year 1979. The mean concentrations were discharge-weighted. Statistical data treatments like correlation matrix and principal component analysis (PCA) were done using RStudio software (CRAN, the Comprehensive R Archive Network, version 3.5.1, RStudio, Inc., Boston, MA, USA). PCA was performed on raw data transformed with log-ratio data using the “rgr” package. The detection of the change-points was calculated using the Buishand test [100,101]. Due to non-normal distribution of the data: (i) trends were determined using the Mann Kendall trend test on linear regression and (ii) the degree of association between two variables was evaluated by the Spearman’s correlation coefficient. Plotting for ternary diagram (Piper diagram, [102]) was performed using the method developed by Hamilton [103].

3. Results

3.1. Stream Water Physico-Chemical Characteristics

3.1.1. Hydrochemical Composition of the Baget Stream Water

The hydrochemical properties are reported in Table 1. All available data from 1978 to 2018 were considered in the Sections 3.1 and 3.1.1 whereas the others sub-sections only concerned the dataset from the period October 1994 to September 2006, plus October 2016 to September 2018 (N = 592). This allowed to homogenize the periods of time studied since the parameters had different sampling frequencies. The values show averages with a 95% confidence interval ($\pm 2\sigma$).

Table 1. Comparison of the main physico-chemical parameter characteristics of the Baget stream water for the two periods: 1978–2018 (first number) versus 1994–2006 plus 2016–2018 (second number), both periods separated by a slash, respectively. Max., maximum; Min., minimum, Std. Dev., standard deviation; CV, coefficient of variation (σ/\bar{X}). The units are $\text{m}^3\cdot\text{s}^{-1}$ (Q, discharge), $^{\circ}\text{C}$ (T° , air temperature), $\mu\text{S}\cdot\text{cm}^{-1}$ (Cond, conductivity), $\text{meq}\cdot\text{L}^{-1}$ (major elements), $\text{mg}\cdot\text{L}^{-1}$ (TDS) and atm (pCO_2). The mean concentrations are discharge-weighted. SIc is the calcite saturation index.

Parameter	N	Max.	Min.	Mean (\bar{X})	Median	Mode	Std. Dev. (σ)	CV
Q	14609/592	10.10/5.41	0.02/0.04	0.44/0.39	0.22/0.20	0.13/0.15	0.67/0.54	1.52/1.40
Air T°	14604/592	29.5/28.2	−11.1/−5.0	12.0/12.2	11.9/12.0	9.2/8.4	6.33/6.35	0.53/0.52
pH	1506/592	8.4/8.4	6.5/6.9	7.7/7.7	7.7/7.7	7.6/7.7	0.18/0.18	0.02/0.02
Cond	637/381	398/398	223/268	306/317	307/316	319/319	24.90/18.97	0.08/0.06
Ca^{2+}	1504/592	3.65/3.55	2.40/2.57	2.97/3.03	2.96/3.01	3.00/3.15	0.18/0.17	0.06/0.05
Mg^{2+}	1504/592	0.75/0.75	0.23/0.23	0.36/0.37	0.36/0.36	0.34/0.40	0.05/0.06	0.13/0.15
Na^{+}	880/592	0.07/0.06	0.03/0.03	0.05/0.05	0.05/0.05	0.05/0.05	0.01/0.00	0.11/0.10
K^{+}	880/592	0.19/0.04	0.00/0.00	0.01/0.01	0.01/0.01	0.01/0.01	0.01/0.00	0.57/0.28
HCO_3^{-}	1501/592	4.40/3.66	2.43/2.57	2.90/2.98	2.88/2.96	2.76/2.76	0.22/0.19	0.07/0.06
SO_4^{2-}	763/592	0.84/0.78	0.01/0.04	0.35/0.35	0.34/0.34	0.27/0.27	0.13/0.13	0.37/0.36
Cl^{-}	893/592	0.25/0.13	0.00/0.02	0.05/0.05	0.05/0.05	0.04/0.04	0.01/0.01	0.27/0.23
NO_3^{-}	705/592	0.17/0.17	0.00/0.00	0.03/0.03	0.03/0.03	0.03/0.03	0.02/0.02	0.57/0.56
TDS	642/592	331.5/327.5	229/229	272.8/273.6	272.0/272.8	264.3/264.3	15.02/14.41	0.06/0.05
pCO_2	1498/592	$1 \times 10^{-1.64}$ / $1 \times 10^{-1.68}$	$1 \times 10^{-3.23}$ / $1 \times 10^{-3.23}$	$1 \times 10^{-2.45}$ / $1 \times 10^{-2.48}$	$1 \times 10^{-2.50}$ / $1 \times 10^{-2.52}$	$1 \times 10^{-2.44}$ / $1 \times 10^{-2.50}$	0.002/0.001	0.53/0.46
SIc	1482/592	0.78/0.78	−0.88/0.64	0.03/0.09	0.03/0.07	0.03/0.04	0.18/0.18	6.09/2.12

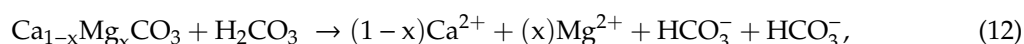
To ensure the consistency of common parameters, the averages were compared for the two studied periods (Table 1). It could be noted that the average and median values for the physico-chemical parameters were similar, with an average variation always less than 5% for almost all the considered parameters. The exception was mainly for discharge (Q) whose mean value decreased from 0.44 to 0.39 $\text{m}^3\cdot\text{s}^{-1}$ and the calcite saturation index (SIc) which increased from 0.03 to 0.09, comparing the whole period (1978–2018) to the 1994–2006 plus 2016–2018 period, respectively.

As a whole, Q exhibited a high variability (coefficient of variation (σ/\bar{X}), CV = 1.52) compared to the variability in air temperature (T° , CV = 0.53), sulfate (SO_4^{2-} , CV = 0.37), partial pressure of CO_2 (pCO_2 , CV = 0.53), magnesium (Mg^{2+} , CV = 0.13), alkalinity (HCO_3^{-} , CV = 0.07), and calcium (Ca^{2+} , CV = 0.06).

Over the whole period, Q and T° values registered daily in BC were in the range of 0.02 to 10.10 $\text{m}^3\cdot\text{s}^{-1}$ and −11.1 to 29.5 $^{\circ}\text{C}$, respectively. Stream water pH averages 7.7 ± 0.4 and the conductivity varied from 223 to 398 $\mu\text{S}\cdot\text{cm}^{-1}$.

The total dissolved solid content ($\text{TDS} = (\text{Ca}^{2+}) + (\text{Mg}^{2+}) + (\text{Na}^{+}) + (\text{K}^{+}) + (\text{HCO}_3^{-}) + (\text{SO}_4^{2-}) + (\text{Cl}^{-}) + (\text{NO}_3^{-}) + (\text{H}_4\text{SiO}_4)$) varies from 229 to 331.5 $\text{mg}\cdot\text{L}^{-1}$, with a mean value of $273 \pm 30 \text{ mg}\cdot\text{L}^{-1}$. The relative abundance of each ion or group of ions (ex: monovalent or divalent cations) can be expressed as the percentage of the total respective sum of cations or anions in equivalents per liter (Figure S1). Whatever the season and the hydrological conditions, the stream water chemistry was

dominated by calcium and alkalinity (mainly corresponding to bicarbonate), which are controlled by carbonate dissolution as follows:



Calcium was the most abundant cation with a concentration varying from 2.40 to 3.65 meq·L⁻¹, i.e., 80.1–92.0% of the sum of cations. The second most important one was Mg²⁺ with a mean value of 0.36 ± 0.10 meq·L⁻¹.

Then, the mean Ca²⁺/Mg²⁺ equivalent ratio was 8.4 ± 1.8. This ratio in Baget was higher than in the Beipanjiang River (3.6) from the Asian Karts Region [70], in the Herault River (2.5) from southern France [104], in the Alpine region (3.7 ± 2.8) [105], in the Ibrahim River–Lebanon (5.8) [106], and exceeded the average value of the world's carbonate basins (4.4) [4]. Nevertheless, it was lower than in the springs of the karstic area of the Jura Mountains (22) in France [34] or in the La Sigouste River (54 ± 39) from the French Southern Alps [107]. In any case, it was rather consistent with the mean value proposed by Meybeck [4] for the French monolithologic basins draining carbonate rocks (12).

Likewise, HCO₃⁻ was the most abundant anion (75.5–99.6% of total anions) with a mean concentration of 2.90 ± 0.42 meq·L⁻¹, while SO₄²⁻ varies from 0.01 to 0.84 meq·L⁻¹. In addition, the equivalent ratio of Ca²⁺ + Mg²⁺ to HCO₃⁻ + SO₄²⁻ was close to a constant value of 1 (1.02 ± 0.06 N = 734). The SO₄²⁻/HCO₃⁻ equivalent ratio was more variable and ranged from 0 to 0.29 and exhibits a mean value of 0.12 ± 0.10 (N = 735), indicating during some hydroclimatic conditions that the stream water was slightly enriched in SO₄²⁻.

Concentrations of sodium and potassium were much lower, with mean values of 0.05 ± 0.01 and 0.01 ± 0.00 meq·L⁻¹, respectively. Chloride and nitrate ions exhibited also low concentrations, with mean values of 0.05 ± 0.01 and 0.03 ± 0.02 meq·L⁻¹, respectively. The respective contribution of these strong acid anions did not exceed 6.5% of the total anions.

The pCO₂ in stream water, which was mainly a function of organic matter degradation and soil respiration, varied from 1 × 10^{-3.23} to 1 × 10^{-1.64} atm with a mean of 1 × 10^{-2.45} atm. The highest pCO₂ values are during low water flow period from June to October. Stream water pCO₂ was always higher than the atmospheric pCO₂ (1 × 10^{-3.5}). SI_c varied in the range of -0.88 to 0.78, and 57% of the samples had SI_c > 0. Moreover, SI_c in BC was lower in the dry season than in the wet season.

3.1.2. Multivariate Statistical Analysis

The principal component analysis (PCA, Figure 2) sets the studied variables according to factors explaining their relative variations [108]. The correlation between the variable and the factor was indicated by a factor loading varying from 1 (strong positive correlation) to -1 (strong negative correlation) [109]. In order to improve the representation of the variables in the PCA, it was decided to consider only 11 variables, the least ones autocorrelated and representative of the hydrochemical processes in the BC. Thus, for example, neither pH nor SI_c were considered in the PCA, both strongly correlated with pCO₂ (see Equations (10) and (11)), or the TDS which was significantly correlated with Ca²⁺ and HCO₃⁻, these two ions representing more of the 75% of TDS. The results of PCA are presented in Figure 2, Tables S1 and S2.

The percentage of variance in the data explained by the first four axes was 83.6%. The first axis (Table S1), responsible for 42.6% of the variance, contrasted Ca²⁺ (87% of contribution to this axis), air temperature (79%), HCO₃⁻ (74%), Na⁺ (68%), Mg²⁺ (60%), and SO₄²⁻ (30%) on the upper positive side of the PCA biplot, with NO₃⁻ (40%) and discharge Q (17%) positioned in the lower negative side.

The second axis (Tables S1 and S2), which extracted 18.9% of the variance, contrasted Q (76%) and HCO₃⁻ (14%) in the right-hand side with SO₄²⁻ (53%), NO₃⁻ (37%), and Mg²⁺ (16%) positioned in the left-hand side. This distribution is reinforced by the positive correlation between Q and HCO₃⁻ and the negative one between SO₄²⁻ and Mg²⁺ (Table S2), suggesting that during low-water level period, SO₄²⁻ and Mg²⁺ concentrations increased, while HCO₃⁻ decreased. Also, Ca²⁺ with HCO₃⁻ on one

side and Mg^{2+} with SO_4^{2-} on the other side, appeared in opposite position relatively to Axis 2 in the PCA plot (Figure 2a, Table S1).

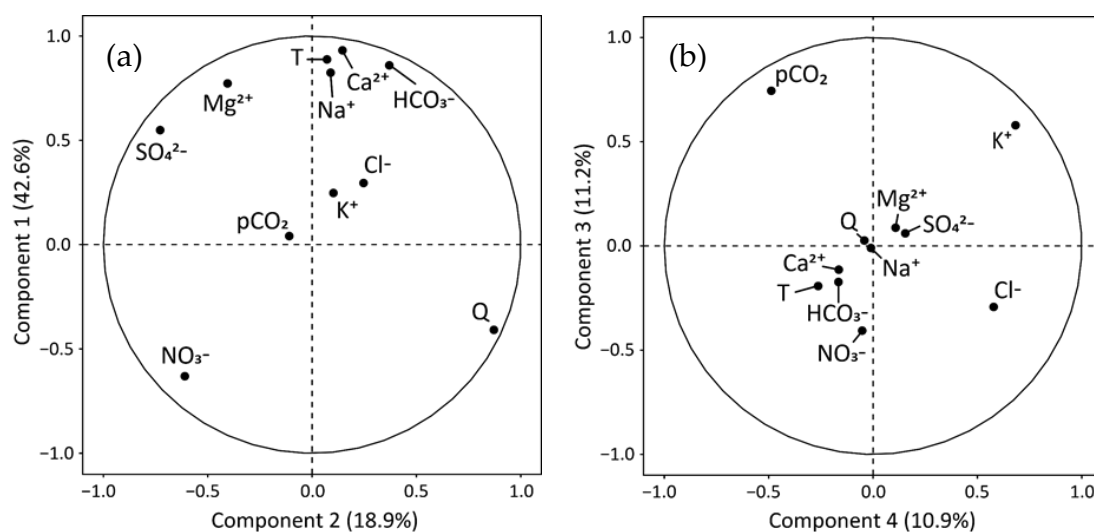
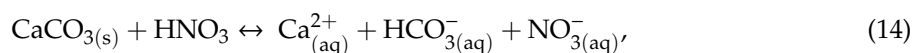


Figure 2. Principal component analysis (PCA) of the main hydrologic and physico-chemical parameters measured in the Baget stream waters for the period 1994–2006 plus 2016–2018 of common measurements (N = 594): (a) components 1 vs. 2 and (b) components 3 vs. 4.

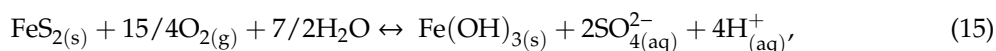
The third axis (Figure 2b and Table S1) accounted for 11.2% of the variance (Table S2). It opposed pCO₂ (55%) and K⁺ (34%) with NO₃⁻ (16%), meanwhile the fourth axis, contributing 10.9% to the variance, contrasted K⁺ (47%) and Cl⁻ (33%) with pCO₂ (24%). Besides, Cl⁻ exhibited a positive correlation with K⁺ and NO₃⁻ (Table S2).

3.1.3. Alkalinity Decrease (Δ_{Alk})

When the main lithology of a catchment is composed of carbonate rocks, the natural dissolution of carbonate by carbonic acid (see Equation (4)) led to an equivalent ratio $\text{Ca}^{2+} + \text{Mg}^{2+}/\text{HCO}_3^-$ of 1 since for two equivalent of calcium, two equivalents of bicarbonate were released, one coming from the soil CO₂ and the other one from the calcite. However, if the carbonate is dissolved by strong acids such as H₂SO₄ (see Equation (13)) or HNO₃ (see Equation (14)), all the bicarbonates released in solution originated from the CO₃ of the minerals as follows:



These strong acids can be supplied by atmospheric acid deposition over the catchment or by pyrite oxidation (Equation (15)) if there are any pyrite minerals in the geological formation:



Then, in calcareous environments, the sulfuric acid released can be rapidly neutralized by carbonate dissolution [110], following the Equation (13). In that case, the equivalent ratio $\text{Ca}^{2+} + \text{Mg}^{2+}/\text{HCO}_3^-$ increases to 2 if the carbonate is only dissolved by the sulfuric acid.

Nevertheless, in the Baget catchment, there is a mixing of carbonate dissolution by carbonic acid and by strong acids like sulfuric acid, releasing sulfates into solution. Finally, the sum $\text{Ca}^{2+} + \text{Mg}^{2+}$ is generally equilibrated by the sum $\text{HCO}_3^- + \text{SO}_4^{2-}$ and thus the equivalent ratio $\text{Ca}^{2+} + \text{Mg}^{2+}/\text{HCO}_3^- + \text{SO}_4^{2-}$ tends to 1.

Consequently, strong acid inputs also result in a decrease of the stream water alkalinity, mainly composed by HCO_3^- [72,111]. This acidification process due to strong acids can be estimated by the decrease of alkalinity. Indeed, the amount of $\text{Ca}^{2+} + \text{Mg}^{2+}$ released by natural dissolution of carbonates by carbonic acid produces a higher alkalinity than that observed (Equation (4)). The decrease of alkalinity (Δ_{Alk} , expressed in equivalent percentage), can be thus calculated as follows for carbonated systems [67]:

$$\Delta_{\text{Alk}} (\%) = \frac{(\text{Ca}^{2+} + \text{Mg}^{2+}) - \text{HCO}_3^-}{(\text{Ca}^{2+} + \text{Mg}^{2+})} \times 100 \quad (16)$$

As seen in Figure 3a, there is a significant positive relationship between $\text{Ca}^{2+} + \text{Mg}^{2+}$ and HCO_3^- in the stream waters of BC but the slope (equivalent ratio) was slightly greater than 1 (Figure 3a), and the cluster of points is above the theoretical line of carbonate dissolution by carbonic acid.

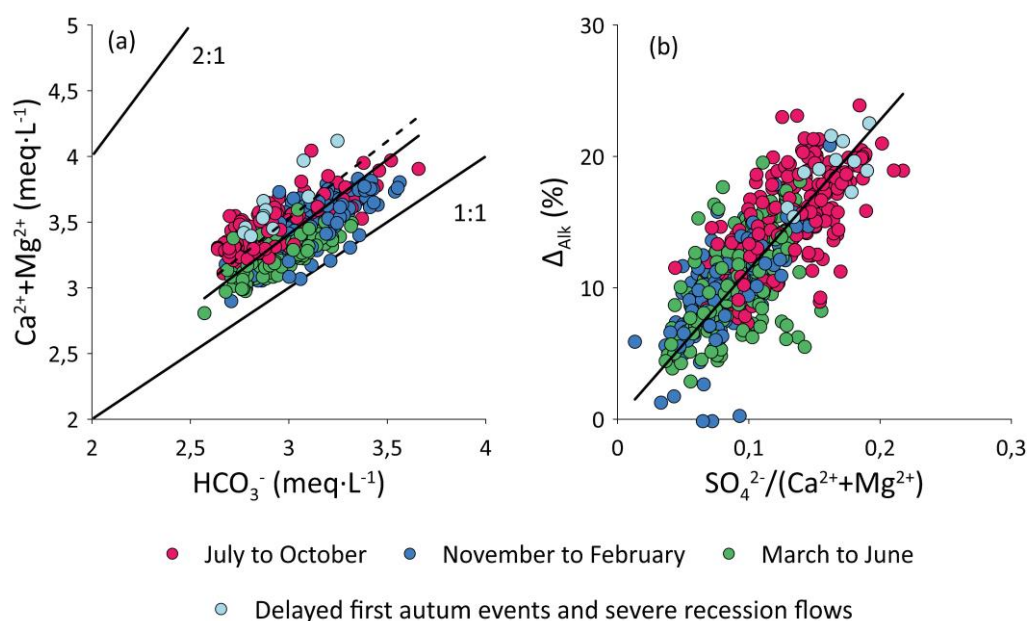
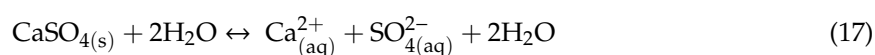


Figure 3. Relationship between (a) $(\text{Ca}^{2+} + \text{Mg}^{2+})$ vs. (HCO_3^-) and (b) alkalinity decrease (Δ_{Alk}) vs. $(\text{SO}_4^{2-})/(\text{Ca}^{2+} + \text{Mg}^{2+})$ equivalent ratio. Regression equations were as follows: (a) the straight line: $y = 1.14x$, $R^2 = 0.98$ ($p \leq 0.001$; $n = 592$) concern all data, the dashed line: $y = 1.18x$, $R^2 = 1.00$ ($p \leq 0.001$; $n = 204$) concern data from July to October, the theoretical lines 2:1 and 1:1 (corresponding to expected $(\text{Ca}^{2+} + \text{Mg}^{2+})/(\text{HCO}_3^-)$ equivalent ratio according to Equations (12)–(14) were indicated; (b) the straight line: $y = 113.8x$, $R^2 = 0.95$ ($p \leq 0.001$ $n = 592$) represent the linear regression for all data. The light blue circles represent flows less than $0.1 \text{ m}^3 \cdot \text{s}^{-1}$ and the first floods of the hydrological year that were delayed in the period between November and December.

Then, the lag observed in Figure 3a could be both attributed to a relative decrease of alkalinity and to a relative increase of $\text{Ca}^{2+} + \text{Mg}^{2+}$ concentration, from theoretical alkalinity and $\text{Ca}^{2+} + \text{Mg}^{2+}$ values corresponding to Equation (4) (line 1/1 in Figure 3a). Nevertheless, the lag observed in Figure 3a could be also attributed to gypsum dissolution as follows:



In order to detect a seasonal and hydrological influence, instantaneous values were gathered into three groups: from July to October (predominantly warm and dry conditions), from November to February (winter time), and from March to June (mainly cold and wet conditions). The summer-autumn group exhibited the highest ratios with a mean slope of 1.18 for the regression (dashed line on Figure 3a; $p \leq 0.001$; $n = 204$).

The alkalinity decrease due to strong acids and to gypsum dissolution was correlated with the SO_4^{2-} to $\text{Ca}^{2+} + \text{Mg}^{2+}$ equivalent ratio, with an average Δ_{Alk} of $15.2 \pm 7.5\%$ which corresponds to an average ratio of 0.13 ± 0.07 (Figure 3b). Thus, as this ratio increased, the Δ_{Alk} also increased, reaching 24% when the ratio was close to 0.2. These highest Δ_{Alk} values were associated with the highest equivalent ratios between $\text{Ca}^{2+} + \text{Mg}^{2+}$ and HCO_3^- (Figure 3a), also displayed mainly between July and October (red points). On the opposite, the lowest Δ_{Alk} values were observed during the winter (blue points) and spring (green points) periods.

3.2. Long Term Trends in Stream Water Chemistry: Instantaneous Values and Mean Annual Data

Long-term trends of the dissolved elements at the outlet of BC for both instantaneous (Figure 4) and mean annual values (Figure 5) were considered to elucidate their behavior over time and their control by environmental factors.

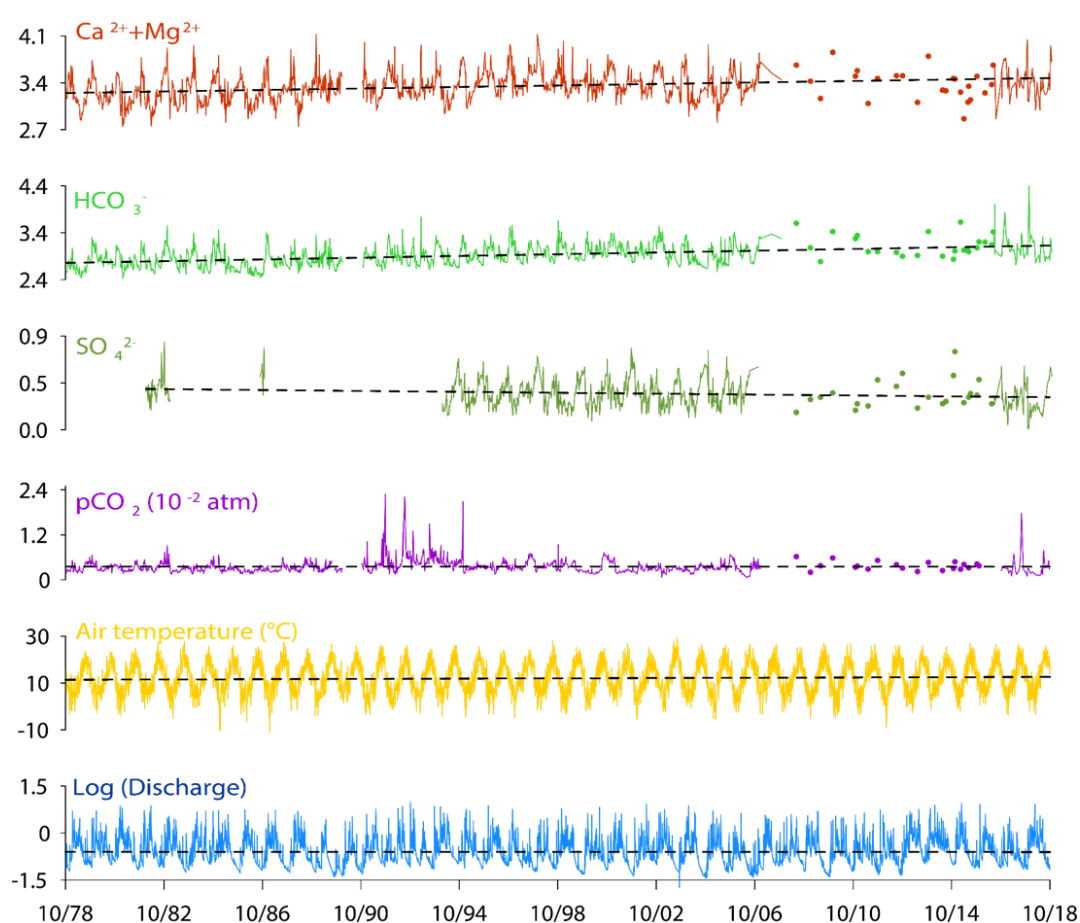


Figure 4. Long-term variations of instantaneous values for $(\text{Ca}^{2+} + \text{Mg}^{2+})$, HCO_3^- , and SO_4^{2-} concentrations ($\text{meq}\cdot\text{L}^{-1}$), pCO_2 (1×10^{-2} atm), air temperature ($^{\circ}\text{C}$), and log of discharge ($\text{m}^3\cdot\text{s}^{-1}$) for the Lachein stream water in the Baget catchment over the period 1978–2018 (data from Binet et al. [82] until 2006 for $(\text{Ca}^{2+} + \text{Mg}^{2+})$, HCO_3^- , and SO_4^{2-} , and this study for the rest). Dotted lines represent the regression lines of the long-term trends. For details of linear regressions, Mann Kendall trend tests and 5-year annual moving average are reported in Tables S3 and S4.

Over the whole 40 years, the air temperature, $\text{Ca}^{2+} + \text{Mg}^{2+}$ and HCO_3^- trends slightly increased, meanwhile the discharge and the pCO_2 trends are not significant (Table S3). The moving averages, which allow to smooth the seasonal variations [112], exhibit the same trends. The two statistical tests applied on these trends (Mann Kendall trend test and linear regression of instantaneous values) were only significant ($p < 0.01$) for temperature, $\text{Ca}^{2+} + \text{Mg}^{2+}$ and HCO_3^- (Table S4).

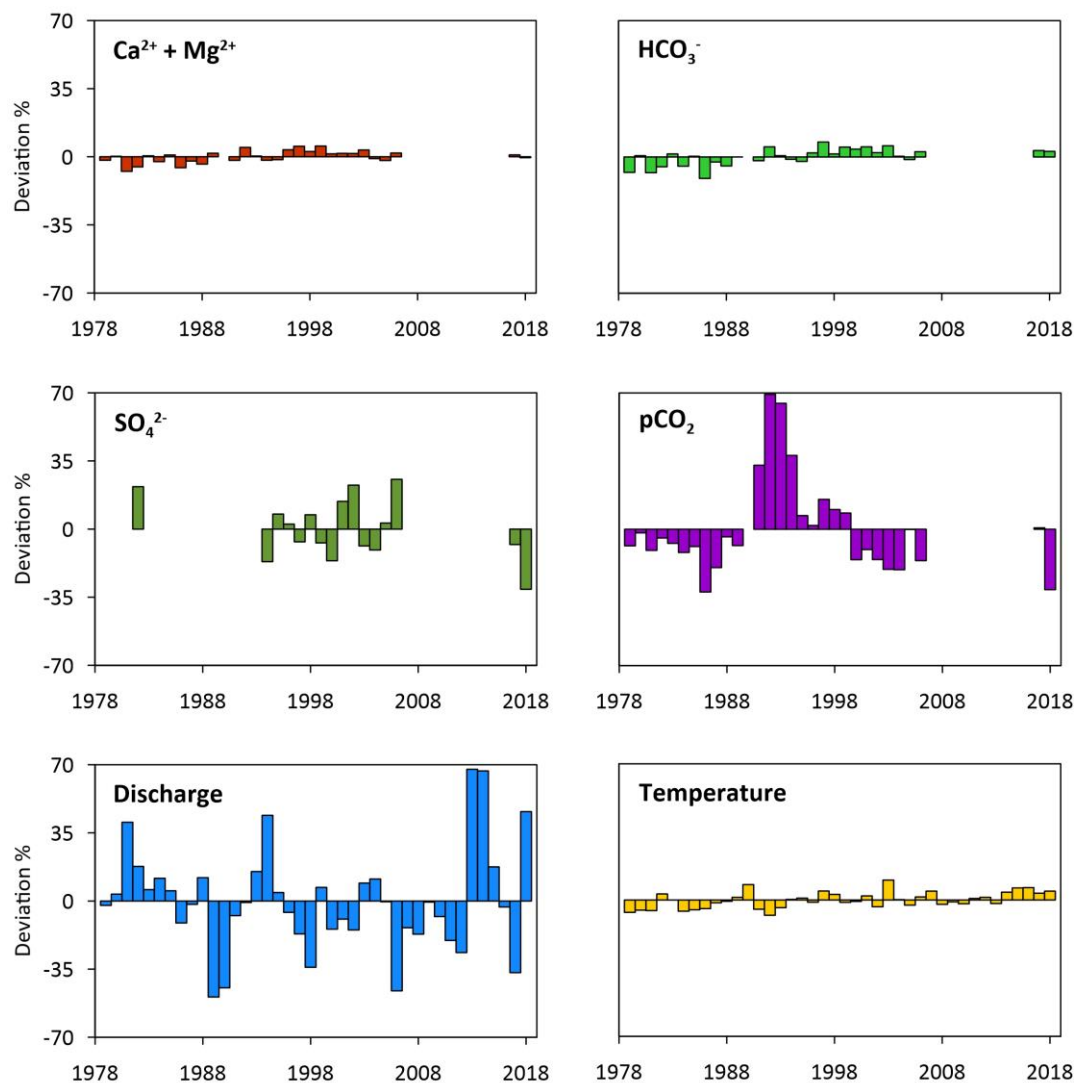


Figure 5. Deviation (in %, $100 \times (y_i - \bar{y})/\bar{y}$) of the mean annual values from the mean interannual values for ($\text{Ca}^{2+} + \text{Mg}^{2+}$), bicarbonate, and sulfate concentrations ($\text{meq}\cdot\text{L}^{-1}$), pCO_2 (atm), discharge ($\text{m}^3\cdot\text{s}^{-1}$), and air temperature ($^{\circ}\text{C}$). The mean concentrations are discharge-weighted. For more details see Table S5.

During the period 1978–2006, similar increasing trends were observed for air temperature, $\text{Ca}^{2+} + \text{Mg}^{2+}$ and HCO_3^- . On the opposite, discharge and SO_4^{2-} concentrations decreased (Table S3). Similarly, as for the longest time period, these trends were only significant ($p < 0.01$) for temperature, discharge, $\text{Ca}^{2+} + \text{Mg}^{2+}$, and HCO_3^- (Table S4).

The Buishand test performed on instantaneous values evidenced the common ruptures in the time series (Table S4). Concerning $\text{Ca}^{2+} + \text{Mg}^{2+}$, a breaking point was observed in September 1988, just following a breaking point for discharge in July 1988, at the beginning of the driest period of the whole series: 1988–1989 ($0.22 \text{ m}^3\cdot\text{s}^{-1}$, deficit of 49% compared to the inter-annual average) and 1989–1990 ($0.24 \text{ m}^3\cdot\text{s}^{-1}$, deficit of 45% compared to the inter-annual average). Regarding HCO_3^- , the breaking point was in October 1991 and occurred six months after the breaking point of pCO_2 in the same year. All these breakpoints are in the period of the pumping test carried out in 1990.

Looking at the mean annual values over the study period, as shown by the deviation to the interannual mean (Figure 5), the air temperature showed an increasing trend with the lower values at the beginning of the survey period (1978–1981, 1983–1986, and 1990–1993), while the highest temperatures were registered at the middle and end of the period (1989–1990, 2002–2003, and 2014–2018). Furthermore,

the discharge displayed a succession of dry periods (1988–1990, 1997–1998, 2005–2006, and 2016–2017) with a mean discharge of $0.25 \text{ m}^3 \cdot \text{s}^{-1}$, deficit of 43% compared to the inter-annual average) and humid ones (1980–1981, 1993–1994, 2012–2014, and 2017–2018) with a mean discharge of $0.67 \text{ m}^3 \cdot \text{s}^{-1}$, increase of 52% compared to the inter-annual average).

Additionally, the three strongest flood events over the whole period were recorded (in decreasing order of mean daily discharge) in October 1993 ($10.10 \text{ m}^3 \cdot \text{s}^{-1}$), February 2015 ($8.94 \text{ m}^3 \cdot \text{s}^{-1}$) and May 2002 ($8.54 \text{ m}^3 \cdot \text{s}^{-1}$). Regarding the temperature, the highest daily air temperature was observed in August 2003 (29.5°C). Furthermore, even if there is no clear relationship between pCO_2 , discharge and temperature, pCO_2 showed the highest values during humid periods with low temperature (1990–1994), the highest one being in October 1991 ($1 \times 10^{-1.64} \text{ atm}$).

3.3. Seasonal Patterns Based on Long Term Data Series in Stream Water Chemistry

The seasonal variations of discharge, temperature, pCO_2 and the dynamics of ion concentrations throughout the year were assessed in Figure 6 using the mean monthly values calculated over the whole period 1994–2006 plus 2016–2018.

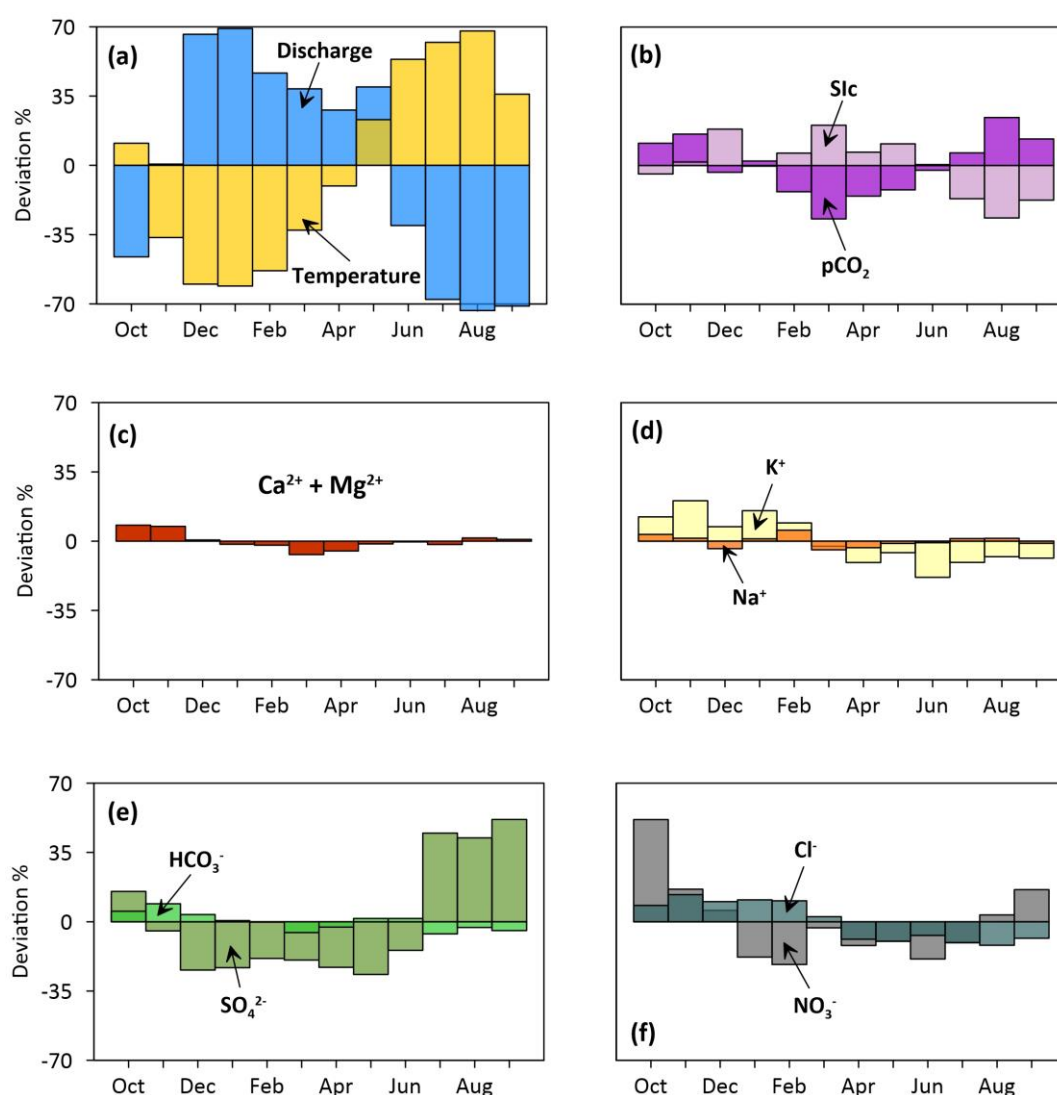


Figure 6. Fluctuation of the mean monthly deviation (in %, $100 \times (y_i - \bar{y})/\bar{y}$) from the mean interannual monthly values of the different hydrochemical parameters for the period 1994–2006 plus 2016–2018. The mean concentrations are discharge-weighted. For more details see Table S6.

The discharge and air temperature exhibited seasonal patterns which are characteristic of the Pyrenees Mountains [88,113]. The fluctuations of mean monthly discharge deviation from the interannual monthly average showed two high flow level periods: the first and highest one from December to February in winter ($0.66 \text{ m}^3 \cdot \text{s}^{-1}$, $5.0 \text{ }^\circ\text{C}$) and a second and lower one between March and May in spring ($0.54 \text{ m}^3 \cdot \text{s}^{-1}$, $11.3 \text{ }^\circ\text{C}$). On the opposite side, the lowest water flow period was from June to October during summer ($0.17 \text{ m}^3 \cdot \text{s}^{-1}$, $19.3 \text{ }^\circ\text{C}$). The air temperature fluctuations presented an exact inverse pattern to discharge (Figure 6a).

Moreover, pCO_2 increased in summer, with the highest average peak in August ($1 \times 10^{-2.42} \text{ atm}$) and it began to decrease slowly in autumn reaching its minimum average peak in March ($1 \times 10^{-2.64} \text{ atm}$). Inversely, spring waters were in equilibrium or undersaturated with respect to calcite at the end of summer and oversaturated with respect to calcite the rest of the year with the highest average peak in March (Figure 6b), corresponding to the lowest mean pCO_2 .

Regarding major elements, K^+ and Cl^- concentrations were higher during the rainy period in winter and decreased as summer approaches (Figure 6d,f, respectively). Conversely, NO_3^- and SO_4^{2-} showed a different pattern with low concentrations during both high flow periods and an accentuated increase in summer especially for SO_4^{2-} (Figure 6e,f).

In addition, $(\text{Ca}^{2+} + \text{Mg}^{2+})$, HCO_3^- , and Na^+ varied slightly during the year (Figure 6c–e, respectively). In fact, $(\text{Ca}^{2+} + \text{Mg}^{2+})$ and HCO_3^- exhibited the maximum concentrations at the end of autumn (October and November), meanwhile, the lowest concentrations occurred in spring for $(\text{Ca}^{2+} + \text{Mg}^{2+})$ and in summer for HCO_3^- .

4. Discussion

4.1. Natural vs. Anthropogenic Sources of Elements

To elucidate the export dynamics of major ions, we analyzed in detail their origin and each of the factors that could influence the export patterns of the major elements in BC.

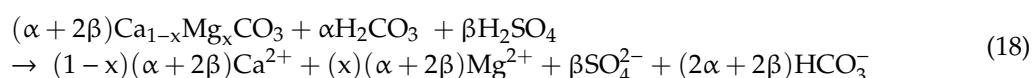
The dissolved elements in stream water result of the interaction between the anthropogenic activities, the atmospheric deposition, the biosphere, the soils and the chemical weathering of rocks and sediments [114].

The natural weathering process due to the reaction of the carbonic acid on minerals, provides dissolved elements such as Ca^{2+} , Mg^{2+} , Na^+ , K^+ , HCO_3^- , and SO_4^{2-} . These elements originate mainly from the dissolution of silicates, carbonates, and sometimes from evaporite dissolution or from the pyrite oxidation [115–118]. This is evidenced in the BC stream waters by the distribution of these dissolved elements along the Factor 1 in the PCA (Figure 2a). According to the major lithology of BC (Figure 1), the main source of Ca^{2+} and HCO_3^- is the calcite dissolution (Equation (2)), these two dominant ions (Figure S1) being strongly positively correlated (Figure 2a, Table S1). Dolomite and magnesian calcite dissolutions are part of the origin of Mg^{2+} [83], however a positive correlation linked Mg^{2+} and SO_4^{2-} (Table S1 and Figure 2). This relationship is related to their higher relative contribution for both elements during the summer period (Figure 6c,e), but only the first one would come from carbonates (Figure 1).

Indeed, sulfate in stream water may have several origins. According to the different lithologies in the basin, two minerals can be sources of sulfate. The first one is gypsum (CaSO_4), which dissolution produces Ca^{2+} and Mg^{2+} , respectively, but does not produce HCO_3^- . A gypsum origin must be taken into account since although the gypsum outcrop is only about 0.2% [83,85], its dissolution remains still possible due to its very high solubility, even after the calcite and dolomite reach saturation [27]. The second mineral is pyrite (FeS_2), whose oxidation produces sulfuric acid (see Equation (15)). The pyrite presence in limestones and schists is confirmed by Bakalowicz [83] and Debroas [85]. Many authors have mentioned that sulfuric acid can substitute carbonic acid in the dissolution of carbonates [70,76,107,119]. This substitution can be proposed as a hypothesis because of the relative decrease in HCO_3^- during summer whereas the SO_4^{2-} concentration increases during low water

period (Figure 6e) as illustrated also by the PCA factor 2 (Figure 2). However, one must also keep in mind that another hypothesis can be put forward: the higher relative contribution of enriched-sulfur sources at the outlet during the summer period compared to high water conditions. This might also explain this relative balance between HCO_3^- and SO_4^{2-} (see Section 4.2).

Indeed, the influence of sulfuric acid on the dissolution of carbonate could be demonstrated by the molar ratio $\text{Ca}^{2+} + \text{Mg}^{2+}$ over HCO_3^- slightly greater than 0.5 (Figure 3a). It indicates that: (1) some $\text{Ca}^{2+} + \text{Mg}^{2+}$ comes from the gypsum dissolution, but also (2) some carbonate dissolution could be induced by sulfuric acid. Therefore, because both sulfuric and carbonic acids are weathering actors in BC, the new weathering equation would be as follows [39]:



This equation is under alkaline conditions and it is pH-dependent process [120]. Also, when bicarbonate ions released will be exported downstream, a significant amount could be transformed to dissolved CO_2 if the pH of stream waters decreases downstream [121].

The influence of sulfuric acid on carbonate dissolution and the gypsum dissolution are both supported by the significant positive correlation between the alkalinity decrease and the relative sulfate content in the Baget stream water (Figure 3b). Nevertheless, during the low water period (Figure 7a,b and Figure 8a), the influence of sulfuric acid on carbonate dissolution is consistent with: (i) the increase of sulfate and the slightly lower pH values in the stream water and (ii) the opposite ratio $\text{Mg}^{2+}/\text{Ca}^{2+}$ pattern observed between HCO_3^- and SO_4^{2-} indicating an enhanced dolomite dissolution, which is less soluble than calcite. Moreover, the increase of carbonate dissolution by sulfuric acid during summer causes an undersaturation of stream waters regarding calcite (Figure 8b).

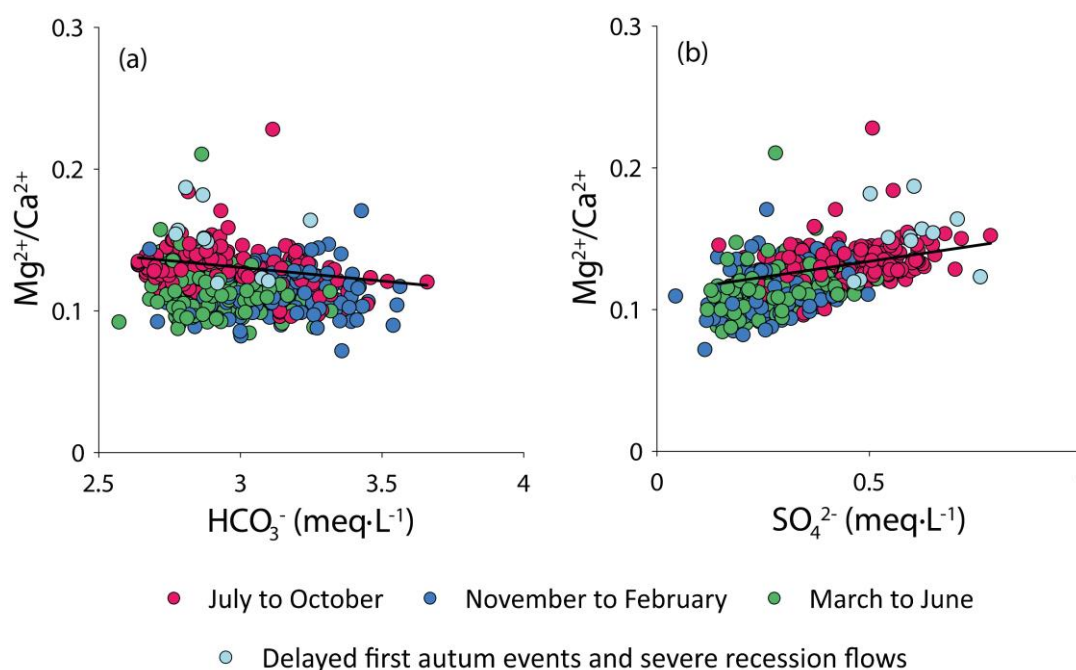


Figure 7. Relationship between the equivalent ratio of $\text{Mg}^{2+}/\text{Ca}^{2+}$ and the concentration of: (a) HCO_3^- and (b) SO_4^{2-} in stream-water. Regression lines represent the equations for the summer period (red points); (a): $y = -0.02x + 0.19$, $R^2 = 0.08$ ($p \leq 0.001$; $n = 204$) and (b): $y = 0.04x + 0.11$, $R^2 = 0.12$ ($p \leq 0.001$; $n = 204$). The light blue circles represent flows less than $0.1 \text{ m}^3 \cdot \text{s}^{-1}$ and the first floods of the hydrological year that were delayed in the period between November and December.

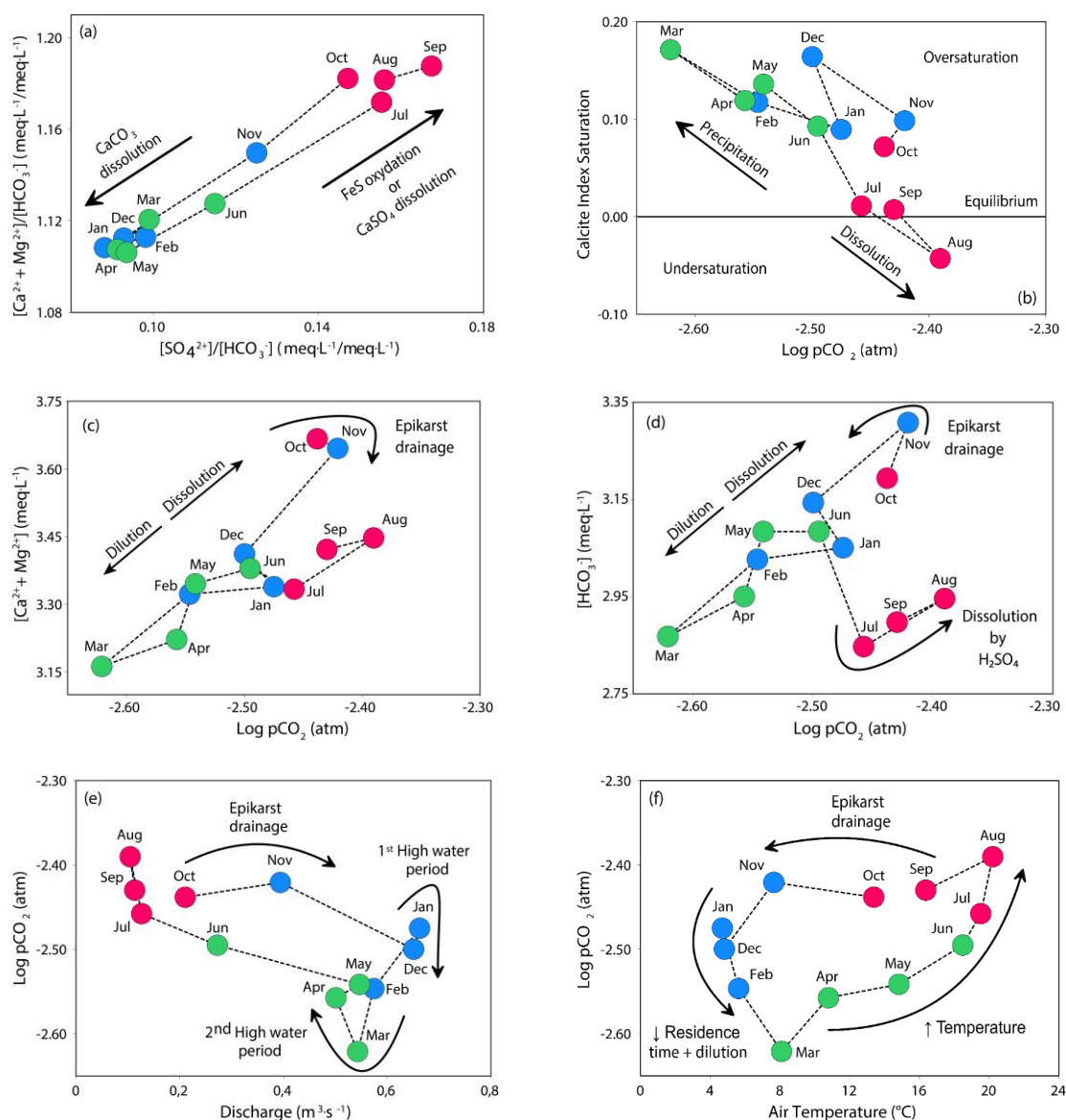


Figure 8. Relationships between interannual mean monthly values of different hydroclimatic and physico-chemical parameters in the Baget stream water for the period 1994–2006 plus 2016–2018: $(\text{Ca}^{2+} + \text{Mg}^{2+})/\text{HCO}_3^-$ ratio versus $\text{SO}_4^{2-}/\text{HCO}_3^-$ ratio (a), SIc, $\text{Ca}^{2+} + \text{Mg}^{2+}$ and HCO_3^- vs. pCO_2 (respectively (b), (c) and (d)), pCO_2 versus discharge (e) and air temperature (f). For more details see Table S6.

Finally, recent results [122] on spatial isotopic analysis of $\delta^{34}\text{S}_{\text{SO}_4}$ carried out on spring and stream waters during summer 2019 based on the lithology of their sub-catchments, give arguments for the major origin of sulfates in stream waters. The presence of sulfate released by pyrite oxidation was detected mainly in waters draining the black flysch ($\delta^{34}\text{S}_{\text{SO}_4} = -8.1\text{‰}$) and the sulfate from gypsum dissolution in waters draining the evaporite clays ($\delta^{34}\text{S}_{\text{SO}_4} = 13.3\text{‰}$). However, the $\delta^{34}\text{S}_{\text{SO}_4}$ isotopic signature of the riverine sulfates ($\delta^{34}\text{S}_{\text{SO}_4} = 11.3\text{‰}$) at the outlet of BC was close to the gypsum signature, showing that sulfate at BC outlet would be mainly supplied by gypsum dissolution [122], even if the contribution of sulfuric acid to carbonate dissolution is higher during the summer period.

Atmospheric deposition is also a potential source of sulfate. The $\delta^{34}\text{S}_{\text{SO}_4}$ in precipitation is unknown in BC but Puig et al. [123] reported values between $+3.3\text{‰}$ and $+0.2\text{‰}$ for Vallcebre (Pyrenees) with a potential atmospheric deposition regional background of 7.2‰ , and Probst A. and Fritz B. (unpublished data, 1994) reported values between $+5.2\text{‰}$ and $+1.8\text{‰}$ for the Strengbach

catchment (Vosges). These data do not allow to discriminate the atmospheric contribution of sulfates for the BC stream waters. However, despite the BC remote position, Binet et al. [82] proposed that a non-negligible part of sulfate would be deposited as dry deposition, particularly by the early sixties. Indeed, some French unpolluted catchments also exhibit high sulfate concentrations [36]. These catchments, which are covered by coniferous forests, were probably also affected by enhanced sulfuric acid inputs due to atmospheric pollution, particularly captured as dry deposits, as already shown for example by Probst et al. [78] and Pierret et al. [124] for the coniferous Strengbach catchment in the Vosges Mountains (France).

After a significant increase until the 1980s, like in other regions in the northern hemisphere [125], acid atmospheric deposition was reduced by half from 1980 to 2005, and has probably decreased at the Baget site like in other sites in France located in remote areas [126]. This might explain the general decreasing trend observed in stream water (SO_4^{2-} (meq·L⁻¹) = -6×10^{-6} (date) + 0.6; $n = 763$; $p < 0.001$ from 1982 to 2018, Figure 4 and Table S3). This trend is very consistent (similar slope) with that observed in the Strengbach stream, which is strongly linked to the decreasing atmospheric sulfates input by precipitation [127].

Even if the atmospheric contribution to riverine sulfate in BC might be lower than the lithological contributions, the long-term influence on carbonate dissolution and CO₂ consumption, has been proved to be non-neglectable at least during the last decades (16–25% of the total Ca²⁺ + Mg²⁺ concentration could have been due to an increase of carbonate dissolution by acid deposition [82]). In addition, sulfuric acid atmospheric deposition decreases during these last decades would have led to stream water Ca²⁺ + Mg²⁺ decrease contrary to what happens, indicating that other processes are involved such as indirect effect of temperature increase or land use change (see Section 4.2).

In the BC, chloride mainly originates from rainfall because there is no anthropogenic activities (such as agriculture) which could supply chloride and there is no evaporitic formation containing halite or sylvite (Figure 1b) [36,128]. This is supported in the PCA (Figure 2b), where this conservative anion is opposed to pCO₂ and Cl⁻ concentration increasing when pCO₂ decreases during the rainy periods. The positive correlation between K⁺ and Cl⁻ (Figure 2a, Table S1), and their joined substantial increase during the rainy season in winter, argue for an atmospheric origin of the two elements, and possibly a soil contribution for K⁺ since it is a largely recycled element not used by vegetation during winter time (Figure 6d,f). Furthermore, Cl⁻ and NO₃⁻ increase in autumn with the first flood events at the beginning of the hydrological year. These high concentrations of Cl⁻ and NO₃⁻, with peaks in October and November, would be due to the onset of rainfall and the leaching of the fir-beech forest or epikarst (see Section 4.3, for NO₃⁻), respectively (Figure 6f) [36].

4.2. Role of Discharge, Temperature and Vegetation on Stream Water Composition and Trends

The hydrological cycle plays a major role in controlling the carbon dynamics in the karst critical zone [129]. The stream discharge, which shows the highest variability during the year, is a key factor in relation to mineral dissolution processes (Equation (4)). Its primary control exerting over fluxes of dissolved elements has long been demonstrated [7,34,37,56,130,131].

However, due to dilution processes, discharge also contributes to concentration decrease. This is mainly due to the input of rainwater and surface runoff, which are less concentrated than groundwater flow [132–134]. This could be illustrated by the decrease in both pCO₂ and ions loads due to high discharge during winter and spring in BC (Figure 8c–e).

In addition, it was observed that the decrease in discharge would lead to an increase in Ca²⁺ and HCO₃⁻ in BC (Figure 6a,c,e). A similar effect was observed on the Houzhai catchment, southwestern China, where a decrease of rainfall between 2007 and 2013 led to an annual mean increase of dissolved element concentrations in stream water [53,129].

Moreover, in BC, during the low water flow period in summer, some tributaries dry out completely, causing particular areas to increase their relative contribution of dissolved elements to the waterbody. An evidence of this process can be supported by the contrast between discharge and Mg²⁺ and SO₄²⁻

on factor 2 in PCA (Figure 2a) and the significant relative increase of SO_4^{2-} in summer (Figure 6e). As evoked before, the change in the relative contribution of water sources can explain the variation of around 10% in Mg^{2+} (coming from dolomitic lithology) and of around 20% in SO_4^{2-} (coming from pyritic lithology) in the piper diagram (Figure S1).

In addition to discharge, the temperature is another factor of similar importance, but with an opposite tendency (Figures 2 and 6a, Table S1). This antagonism related to the climate characteristics of the Pyrenees Mountains (high water flow with lower temperature in winter and early spring, and low water flow with higher temperature during summer and early autumn). It is also supported by the negative relationship between temperature and both Cl^- and K^+ (Figure 2), which are rainfall or vegetation dependent elements.

Indeed, temperature is an important catalytic agent in the dissolution reactions of minerals. However, carbonate dissolution was shown as an exception. The increase in temperature contributes to a decrease in the dissolution because the solubility of calcite increases when temperature decreases [12,98]. In BC, this is opposite to the observed long-term trend patterns of increasing temperature and $\text{Ca}^{2+} + \text{Mg}^{2+}$ and HCO_3^- (Figure 4), indicating the influence of other key factors. Indeed, air temperature is considered as the main factor related to seasonal changes in soil pCO_2 as demonstrated by the nice anti-clockwise hysteresis observed in Figure 8f. In summer, low soil moisture could enhance the diffusion of biogenic CO_2 to the atmosphere and could also limit the growth rate of plants by decreasing their role in the soil [135]. Despite these processes, Zhao et al. [39] showed that the increase in temperature not only improves pCO_2 derived from root respiration, but also stimulates the decomposition of organic matter in the soil. Therefore, the increase in temperature would rise the generation of biogenic CO_2 , which can enhance the dissolution of carbonates. The factor 1 in PCA (Figure 2a) shows this influence, in which the temperature is resembled with SO_4^{2-} but also with Ca^{2+} and HCO_3^- . Additional evidence is shown with the positive relationship between $\text{Ca}^{2+} + \text{Mg}^{2+}$ and HCO_3^- with pCO_2 (Figure 8c,d), denoting that a higher pCO_2 level in water promotes higher carbonate dissolution rates. Figure 8f also shows a net pCO_2 decrease from end-of-summer to winter, probably due to the increase in water flow level and to the decrease of temperature [136,137]. But outside the dilution effect during the high flow period, the lower content of bicarbonate could be attributed to the consumption of DIC by secondary formation of CaCO_3 and also to losses by CO_2 degassing into the atmosphere (inverse reaction of Equation (4)). This hypothesis is supported by a higher SIc and a lower pCO_2 during high flow conditions (Figure 8b) [138]. The lowest pCO_2 values could be also related to a lower residence time during the spring period. After this period, stream water pCO_2 increases again with temperature increase until August. Previous studies showed similar behavior at stream water BC: pCO_2 was $1 \times 10^{-1.9}$ atm in summer and $1 \times 10^{-2.6}$ atm in winter [83].

At the annual and inter-annual scale, it is difficult at this stage (more data in Ulloa-Cedamano PhD in progress) to provide complete evidence that the trends observed for Ca^{2+} and HCO_3^- are mostly related to climate change or land-use change (Figure 5). The observed significant increasing trends over time of $\text{Ca}^{2+} + \text{Mg}^{2+}$ and HCO_3^- (Figure 4) could be explained by the temperature increase ($p < 0.01$) as described above and the discharge decrease ($p < 0.01$ from 1978 to 2006). However, surprisingly, under usual hydroclimatic conditions without extreme events, there is no relationship between pCO_2 level and $\text{Ca}^{2+} + \text{Mg}^{2+}$ and bicarbonates (Figure 5). The pCO_2 peaks observed in the early 1990s could be due to a side effect of the long-term pumping test of 1990 (Figures 4 and 5). At this period, the decrease of the discharge corresponds to a pH decrease. This could be interpreted as: (1) a decrease of the relative contribution of waters draining carbonates and (2) a relative increase of the contribution of waters draining lithological formations containing pyrites. This pH decreases of the water would have caused the transformation of bicarbonate ions into dissolved CO_2 (Equation (19)). In fact, Mangin [79] has shown that a very severe low water flow conditions can impact the hydrological functioning of a karst system for a long period (at least 5 years in the case of Baget).

At the seasonal scale, most of stream waters in BC had SIc above 0 (Figure 8b), indicating that Equation (4) would occur in the opposite direction in response to calcite oversaturation, allowing

calcite precipitation and CO₂ degassing to the atmosphere. Indeed, it has been shown by several studies [38,53,139] based on a theoretical diffusion model of CO₂ fluxes between river waters and atmosphere, that CO₂ evasion is important in the riverine carbon cycle. Conversely, August is the only month showing an undersaturation with regard to calcite and holding the highest pCO₂. In fact, the pCO₂ increase leads to the increase in calcite dissolution needed to reach the equilibrium.

Additionally, pCO₂ of stream water in winter and spring tends towards low values but remaining always greater than the atmospheric pCO₂ ($>1 \times 10^{-3.5}$ atm). This shows that the direct atmospheric CO₂ contribution to DIC can be ignored in BC. At the same time, this could be a clue showing that groundwater stored near the surface in the epikarst could be in relation to a gas phase permanently enriched with the soil pCO₂ [28]. Therefore, the role of epikarst on the dynamics of carbonate dissolution is important to consider.

4.3. Respective Control of Karst and Epikarst on Stream Water Chemical Composition and Trends

The epikarst drives rainwater into a network of drainage pathways [140,141]. During the rainy season, a part of rainwater which recharges the karst aquifer is partly stored in the epikarst causing three different processes: (i) evaporation processes of a large fraction (with concentration of dissolved salts), (ii) slow infiltration through the fine cracks and pores, and (iii) delayed infiltration during the heavy rains recharging the epikarst (“piston effect”) [28,142,143]. These processes can be observed directly and indirectly in BC. For example, all dissolved elements, even SO₄^{2−}, would be concentrated in the epikarst during summer, a period of intense mineralization in the soils. Later, all these major elements subjected to a delayed infiltration by storage near the surface, are released with the first heavy rainfalls in autumn, in particular NO₃[−] (Figures 6f and 8c,d). This “piston effect” may be displayed by the positive correlation between dissolved elements coming from the dissolution of carbonates, mainly calcite (Ca²⁺ and HCO₃[−]) and those coming from rainwater or vegetation interface recycling (Cl[−] and K⁺) (Figure 2, Table S1).

The decrease of sulfate concentrations observed in autumn with the inputs of the first rainfalls, illustrate the contribution of water draining lithological areas less concentrated in sulfate (see November position on Figure 8a). Subsequently, since the pre-stored water in the epikarst has been released in winter, the ions exhibiting the greatest increase are those mainly originating from rainfall (i.e., Cl[−]), or less recycled by the vegetation due to the dormant period (i.e., K⁺) (Figure 6f,d, respectively). Lastly, during the spring, part of rainwater incoming will be used to recharge the epikarst [79] and then, during summer, the epikarst water is progressively mineralized.

The epikarst also appears as a reservoir with higher pCO₂ values than those measured in the surrounding soils and caves, due to an active exchange between the sub-surface flow and deep flow [53], and to a CO₂ accumulation effect [47,144]. Therefore, during the temperature conditions in summer, carbonate dissolution is enhanced by high concentrations of soil CO₂. Then, Ca²⁺ and HCO₃[−] concentrations increase in epikarst aquifers. Afterwards, large amounts of Ca²⁺ + Mg²⁺ and HCO₃[−] can be released during the epikarst drainage in autumn (Figure 8b,c, respectively). Also, the higher exchange between epikarst zone and the atmosphere can be evaluated by the pCO₂ decrease and the calcite oversaturation (SI_c > 0) during the epikarst drainage (Figure 8b).

Lastly, the rise in ion concentrations observed in stream water during autumn with the first stormflow events occurring after the strong summer evaporation period, is supposed to come from soil horizons and epikarst drainage. This “flushing effect” was evidenced by Walling and Foster [145] and later on by several authors on catchment draining various lithologies and under various climate conditions: on silicate basins such as the Mont-Lozère, the Strengbach and Ringelbach [72,111], the silicate-rich Chari–Logone River catchment in Chad [146], the Vantaa River boreal catchment in southern Finland [147], the Heidingzi agricultural catchment in China [137], and also on calcareous basins such as the Oka River forested catchment in Spain [148], the Middle Bussento Karst System in Italy [149], and the Chenqi agricultural karstic catchment [150].

5. Conclusions

This study investigated the response of a small, remote, and forested karst catchment to the impact of inter-annual and seasonal changes on stream water hydrochemistry using a 40-year period survey, through instantaneous, monthly, and annual data series.

Over the long-term, the significant rising trends in $\text{Ca}^{2+} + \text{Mg}^{2+}$ and bicarbonate concentrations could be related to the global warming as shown by the air temperature increase, which enhanced the biogenic activity and then the carbonate dissolution. Whereas discharge and pCO_2 trends are not significant, except for discharge during the period 1978–2006 (decreasing trend). In contrast, a decreasing trend was observed for sulfates, which might be related to atmospheric deposition decrease over the last decades. Indeed, in the context of global warming and hydroclimatic fluctuations, the increasing trends of $\text{Ca}^{2+} + \text{Mg}^{2+}$ and bicarbonates could be a consequence of the buffering effect of carbonate dissolution on the global increasing trends of atmospheric CO_2 , and then on short time scales, an important CO_2 sink.

The seasonal patterns allowed to decipher the origin and the export dynamics of major ions in the BC: (i) a major lithological origin for the main base cations (Ca^{2+} and Mg^{2+}) and anions (bicarbonates and sulfates) from carbonates and/or sulfate mineral dissolution; (ii) a major atmospheric origin for chloride and potassium, and (iii) a biological origin for nitrates. Besides, calcite undersaturation and carbonate dissolution increase were observed during the warm climatic conditions and low flow period, in relation with the biogenic CO_2 production.

Outside the classical controls of water–rock interactions (depending on water residence time), dilution effect (by precipitation input), and concentrating effect (by evapotranspiration output), the water discharge regime induces a variable importance of water source contribution from the different lithologies. This is illustrated by the increased sulfate to bicarbonate ratio up to two-times higher during low water flow period. Moreover, the role of the epikarst contribution was highlighted, and particularly illustrated by the first heavy rains in autumn, which cause by “piston effect” and “flushing effect”, the release of large amounts of $\text{Ca}^{2+} + \text{Mg}^{2+}$ and bicarbonates previously stored in the epikarst solutions.

Such long-term studies of the critical zone must be promoted since they have proven to be efficient in identifying: water and element sources and trends, weathering and biogeochemical processes, at various time scales, and the key controlling parameters. In a period of contrasting regional climate patterns, such critical zone survey provides robust validation data for the development of predictive models.

Supplementary Materials: The following are available online at <http://www.mdpi.com/2073-4441/12/5/1227/s1>, Figure S1: Piper ternary diagram for major ion concentrations in Baget stream waters for the period from 1994 to 2006 and 2016 to 2018, Table S1: Principal Component Analysis (PCA). Contribution of the main physico-chemical parameters and discharge to the four first PCA factors (in %, $N = 592$). In bold the percentages greater than 10. The signs (+) or (−) indicate positive and negative correlation, respectively, Table S2: Eigenvalues relative to the 10 main axis of the PCA ($N = 594$), Table S3: Regression coefficients (a and b) for the linear trends ($Y = aX + b$) for the main hydrochemical parameters over the periods 1978–2018 (all elements, except sulfates, 1982–2018) and 1978–2006 (all elements, except sulfates, 1994–2018). p -value: significance level, R^2 : Pearson correlation coefficient, N : number of observations (in the calculations, X was expressed in days from 01-01-1900), Table S4: Change-points (according to Buishand tests), statistical trend test (Mann Kendall trend tests and linear regression test for instantaneous, mean monthly and mean annual values) as well as on 5-year annual moving average, for the main physico-chemical parameters over the considered study periods. p -values were lower than 0.01, except when p -values were mentioned. The sign (+) and (−) indicated a positive or negative trend, respectively, Table S5: Mean annual values of the physico-chemical parameter characteristics of the Baget stream water for the period 1978–2018. The units are $\text{m}^3 \cdot \text{s}^{-1}$ (Q, discharge), $^{\circ}\text{C}$ (T° , air temperature), $\mu\text{S} \cdot \text{cm}^{-1}$ (Cond, conductivity), $\text{meq} \cdot \text{L}^{-1}$ (major elements), $\text{mg} \cdot \text{L}^{-1}$ (TDS), and atm (pCO_2). The mean concentrations are discharge-weighted. SIC is the calcite saturation index. Each hydrological year (H.Y.) starts on 1 October and ends on the next 30 September. Table S6: Mean interannual monthly values of the physico-chemical parameter characteristics of the Baget stream water for the period 1994–2006 plus 2016–2018. The units are $\text{m}^3 \cdot \text{s}^{-1}$ (Q, discharge), $^{\circ}\text{C}$ (T° , air temperature), $\mu\text{S} \cdot \text{cm}^{-1}$ (Cond, conductivity), $\text{meq} \cdot \text{L}^{-1}$ (major elements), $\text{mg} \cdot \text{L}^{-1}$ (TDS), and atm (pCO_2). The mean concentrations are discharge-weighted. SIC is the calcite saturation index. N is the number of samples for each month.

Author Contributions: Conceptualization, F.U.-C., A.P., and J.-L.P.; methodology, F.U.-C., A.P., and J.-L.P.; validation, F.U.-C., A.P., and J.-L.P.; formal analysis, F.U.-C.; investigation, F.U.-C., A.P., and J.-L.P.; resources, F.U.-C., T.C., V.P.-S., and C.P.; data curation, F.U.-C.; writing—original draft preparation, F.U.-C.; writing—review and editing, A.P., J.-L.P., S.B. (Stéphane Binet), M.B., and S.B. (Sandra Béranger); visualization, F.U.-C.; supervision, A.P. and J.-L.P.; project administration, A.P. and J.-L.P.; funding acquisition, A.P. and J.-L.P. All authors have read and agreed to the published version of the manuscript.

Funding: This research was funded by the CNRS INSU-INEE.

Acknowledgments: The authors specially thank the support from CNRS INEE and INSU, SNO KARST, OZCAR, and Zone Atelier Pyrénées-Garonne (LTSER ZA PYGAR). The data of this work were gathered and partly monitored within the framework of the French KARST Observatory Network SNO KARST (www.sokarst.org) initiative of the INSU/CNRS, which aims to strengthen knowledge-sharing and to promote cross-disciplinary research on karst systems. The SNO Karst is also included in the French Research Infrastructure OZCAR, the French network of Critical Zone Observatories. The EcoLab analytical platforms, PAPC (F. Julien, D. Lambrigt, and W. Amblas) and the chemical lab service from the GET (C. Causserand and P. Besson) contribute to the analytical work during the more recent years. F. Ulloa-Cedamano's PhD was supported by a fellowship from the French Ministry of Higher Education, Research and Innovation. Special thanks go to those who helped at a given period in the field for data collection or analytical work: a particular thought goes to Alain Mangin to whom this work is dedicated.

Conflicts of Interest: The authors declare no conflict of interest.

References

- Robertson, G.P.; Paul, E.A.; Harwood, R.R. Greenhouse Gases in Intensive Agriculture: Contributions of Individual Gases to the Radiative Forcing of the Atmosphere. *Science* **2000**, *289*, 1922–1926. [[CrossRef](#)] [[PubMed](#)]
- Guo, J.; Zhou, C. Greenhouse gas emissions and mitigation measures in Chinese agroecosystems. *Agric. For. Meteorol.* **2007**, *142*, 270–277. [[CrossRef](#)]
- Liu, Y.; Wan, K.; Tao, Y.; Li, Z.; Zhang, G.; Li, S.; Chen, F. Carbon Dioxide Flux from Rice Paddy Soils in Central China: Effects of Intermittent Flooding and Draining Cycles. *PLoS ONE* **2013**, *8*, e56562. [[CrossRef](#)] [[PubMed](#)]
- Meybeck, M. Global chemical weathering of surficial rocks estimated from river dissolved loads. *Am. J. Sci.* **1987**, *287*, 401–428. [[CrossRef](#)]
- Gaillardet, J.; Dupre, B.; Louvat, P.; Allegre, C.J. Global silicate weathering and CO₂ consumption rates deduced from the chemistry of large rivers. *Chem. Geol.* **1999**, *159*, 3–30. [[CrossRef](#)]
- Ludwig, W.; Probst, J.-L. Predicting the oceanic input of organic carbon by continental erosion. *Glob. Biogeochem. Cycles* **1996**, *10*, 23–41. [[CrossRef](#)]
- Amiotte-Suchet, P.; Probst, J.-L.; Ludwig, W. Worldwide distribution of continental rock lithology: Implications for the atmospheric/soil CO₂ uptake by continental weathering and alkalinity river transport to the oceans. *Glob. Biogeochem. Cycles* **2003**, *17*. [[CrossRef](#)]
- Ford, D.; Williams, P. *Karst Hydrogeology and Geomorphology*; John Wiley & Sons, Inc.: Hoboken, NJ, USA, 2007; p. 562.
- Chen, Z.; Auler, A.S.; Bakalowicz, M.; Drew, D.; Griger, F.; Hartmann, J.; Jiang, G.; Moosdorf, N.; Richts, A.; Stevanovic, Z.; et al. The World Karst Aquifer Mapping project: Concept, mapping procedure and map of Europe. *Hydrogeol. J.* **2017**, *25*, 771–785. [[CrossRef](#)]
- Meybeck, M. 5.08—Global Occurrence of Major Elements in Rivers. In *Treatise on Geochemistry*; Holland, H.D., Turekian, K.K., Eds.; Elsevier: Pergamon, NY, USA, 2003; Volume 5, pp. 207–223.
- Curl, R.L. Carbon Shifted but Not Sequestered. *Science* **2012**, *335*, 655. [[CrossRef](#)]
- Cao, J.; Yuan, D.; Groves, C.; Huang, F.; Yang, H.; Lu, Q. Carbon Fluxes and Sinks: The Consumption of Atmospheric and Soil CO₂ by Carbonate Rock Dissolution. *Acta Geol. Sin. Engl. Ed.* **2012**, *86*, 963–972.
- Blum, J.D.; Gazis, C.A.; Jacobson, A.D.; Page Chamberlain, C. Carbonate versus silicate weathering in the Raikhot watershed within the High Himalayan Crystalline Series. *Geology* **1998**, *26*, 411–414. [[CrossRef](#)]
- Jacobson, A.D.; Blum, J.D.; Walter, L.M. Reconciling the elemental and Sr isotope composition of Himalayan weathering fluxes: Insights from the carbonate geochemistry of stream waters. *Geochim. Cosmochim. Acta* **2002**, *66*, 3417–3429. [[CrossRef](#)]
- Gombert, P. Role of karstic dissolution in global carbon cycle. *Glob. Planet. Chang.* **2002**, *33*, 177–184. [[CrossRef](#)]
- Liu, Z.; Dreybrodt, W.; Liu, H. Atmospheric CO₂ sink: Silicate weathering or carbonate weathering? *Appl. Geochem.* **2011**, *26*, S292–S294. [[CrossRef](#)]

17. Liu, Z.; Macpherson, G.L.; Groves, C.; Martin, J.B.; Yuan, D.; Zeng, S. Large and active CO₂ uptake by coupled carbonate weathering. *Earth Sci. Rev.* **2018**, *182*, 42–49. [\[CrossRef\]](#)
18. Messerli, B.; Viviroli, D.; Weingartner, R. Mountains of the world: Vulnerable water towers for the 21st century. *Ambio* **2004**, *13*, 29–34. [\[CrossRef\]](#)
19. IPCC. *Climate Change 2007 Synthesis Report. Contribution of Working Groups I, II and III to the Fourth Assessment Report of the Intergovernmental Panel on Climate Change*; Pachauri, P.K., Reisinger, A., Core Writing Team, Eds.; IPCC: Geneva, Switzerland, 2007.
20. IPCC. *Climate Change 2014: Synthesis Report. Contribution of Working Groups I, II and III to the Fifth Assessment Report of the Intergovernmental Panel on Climate Change*; Pachauri, R.K., Meyer, L.A., Core Writing Team, Eds.; IPCC: Geneva, Switzerland, 2014.
21. Viviroli, D.; Archer, D.R.; Buytaert, W.; Fowler, H.J.; Greenwood, G.B.; Hamlet, A.F.; Huang, Y.; Koboltschnig, G.; Litaor, M.I.; López-Moreno, J.I.; et al. Climate change and mountain water resources: Overview and recommendations for research, management and policy. *Hydrol. Earth Syst. Sci.* **2011**, *15*, 471–504. [\[CrossRef\]](#)
22. Beniston, M.; Stoffel, M. Assessing the impacts of climatic change on mountain water resources. *Sci. Total Environ.* **2014**, *493*, 1129–1137. [\[CrossRef\]](#)
23. Morán-Tejeda, E.; Ceballos-Barbancho, A.; Llorente-Pinto, J.M. Hydrological response of Mediterranean headwaters to climate oscillations and land-cover changes: The mountains of Duero River basin (Central Spain). *Glob. Planet. Chang.* **2010**, *72*, 39–49. [\[CrossRef\]](#)
24. López-Moreno, J.I.; Zabalza, J.; Vicente-Serrano, S.M.; Revuelto, J.; Gilaberte, M.; Azorin-Molina, C.; Morán-Tejeda, E.; García-Ruiza, J.M.; Taguec, C. Impact of climate and land use change on water availability and reservoir management: Scenarios in the Upper Aragón River, Spanish Pyrenees. *Sci. Total Environ.* **2014**, *493*, 1222–1231. [\[CrossRef\]](#)
25. López-Moreno, J.I.; Beniston, M.; García-Ruiz, J.M. Environmental change and water management in the Pyrenees: Facts and future perspectives for Mediterranean mountains. *Glob. Planet. Chang.* **2008**, *61*, 300–312. [\[CrossRef\]](#)
26. Szczypta, C.; Gascoin, S.; Houet, T.; Hagolle, O.; Dejoux, J.F.; Vigneau, C.; Fanise, P. Impact of climate and land cover changes on snow cover in a small Pyrenean catchment. *J. Hydrol.* **2015**, *521*, 84–99. [\[CrossRef\]](#)
27. Mokadem, N.; Hamed, Y.; Hfaïd, M.; Dhia, H.B. Hydrogeochemical and isotope evidence of groundwater evolution in El Guettar Oasis area, Southwest Tunisia. *Carbonates Evaporites* **2015**, *30*, 417–437. [\[CrossRef\]](#)
28. Bakalowicz, M. Epikarst. In *Encyclopedia of Caves*, 2nd ed.; Academic Press: Cambridge, MA, USA, 2012; pp. 284–288. [\[CrossRef\]](#)
29. Bakalowicz, M. Karst groundwater: A challenge for new resources. *Hydrogeol. J.* **2005**, *13*, 148–160. [\[CrossRef\]](#)
30. Bakalowicz, M. *The Epikarst, the Skin of Karst*; Karst Waters Institute Special Publication 9: Charles Town, WV, USA, 2003; pp. 16–22.
31. Daher, W.; Pistre, S.; Kneppers, A.; Bakalowicz, M.; Najem, W. Karst and artificial recharge: Theoretical and practical problems. A preliminary approach to artificial recharge assessment. *J. Hydrol.* **2011**, *408*, 189–202. [\[CrossRef\]](#)
32. Raymond, P.A.; Oh, N.-H.; Turner, R.E.; Broussard, W. Anthropogenically enhanced fluxes of water and carbon from the Mississippi River. *Nature* **2008**, *451*, 449. [\[CrossRef\]](#)
33. Jeannin, P.-Y.; Hessenauer, M.; Malard, A.; Chapuis, V. Impact of global change on karst groundwater mineralization in the Jura Mountains. *Sci. Total Environ.* **2016**, *541*, 1208–1221. [\[CrossRef\]](#)
34. Calmels, D.; Gaillardet, J.; François, L. Sensitivity of carbonate weathering to soil CO₂ production by biological activity along a temperate climate transect. *Chem. Geol.* **2014**, *390*, 74–86. [\[CrossRef\]](#)
35. Romero-Mujalli, G.; Hartmann, J.; Börker, J.; Gaillardet, J.; Calmels, D. Ecosystem controlled soil-rock pCO₂ and carbonate weathering—Constraints by temperature and soil water content. *Ann. N. Y. Acad. Sci.* **2018**, *769*, 71–84. [\[CrossRef\]](#)
36. Meybeck, M. Composition chimique des ruisseaux non pollués en France. Chemical composition of headwater streams in France. *Sci. Géol. Bull.* **1986**, *39*, 3–77. [\[CrossRef\]](#)
37. Amiotte-Suchet, P.; Probst, J.-L. Modelling of atmospheric CO₂ consumption by chemical weathering of rocks: Application to the Garonne, Congo and Amazon basins. *Chem. Geol.* **1993**, *107*, 205–210. [\[CrossRef\]](#)
38. Wang, F.S.; Wang, Y.; Zhang, J.; Xu, H.; Wei, X. Human impact on the historical change of CO₂ degassing flux in River Changjiang. *Geochem. Trans.* **2007**, *8*, 1–10. [\[CrossRef\]](#) [\[PubMed\]](#)

39. Zhao, R.; Liu, Z.; Huang, H.; Dong, L. Difference in the relationship between soil CO₂ concentration and the karst-related carbon cycle under different land use types in southwest China. *Carbonates Evaporites* **2019**, *34*, 1569–1581. [\[CrossRef\]](#)
40. Hartmann, J.; Jansen, N.; Dürr, H.H.; Kempe, S.; Köhler, P. Global CO₂-consumption by chemical weathering: What is the contribution of highly active weathering regions? *Glob. Planet. Chang.* **2009**, *69*, 185–194. [\[CrossRef\]](#)
41. Zhong, J.; Li, S.L.; Tao, F.; Yue, F.; Liu, C.Q. Sensitivity of chemical weathering and dissolved carbon dynamics to hydrological conditions in a typical karst river. *Sci. Rep.* **2017**, *7*, 1–9. [\[CrossRef\]](#) [\[PubMed\]](#)
42. Clow, D.W.; Mast, M.A. Mechanisms for chemostatic behavior in catchments: Implications for CO₂ consumption by mineral weathering. *Chem. Geol.* **2010**, *269*, 40–51. [\[CrossRef\]](#)
43. Drever, J.I. *The Geochemistry of Natural Waters, Surface and Groundwater Environments*, 3rd ed.; Prentice-Hal: Upper Saddle River, NJ, USA, 1997.
44. Parkhurst, D.L.; Appelo, C.A.J. *User's Guide to PHREEQC (Version 2): A Computer Program for Speciation, Batch-reaction, One-dimensional Transport, and Inverse Geochemical Calculations*; Geological Survey: Denver, CO, USA, 1999.
45. Zeebe, R.; Wolf-Gladrow, D. *CO₂ in Seawater: Equilibrium, Kinetics, Isotopes*, 1st ed.; Elsevier Oceanography Series: Amsterdam, The Netherlands, 2001.
46. Troester, J.W.; White, W.B. Seasonal Fluctuations in the Carbon Dioxide Partial Pressure in a Cave Atmosphere. *Water Resour. Res.* **1984**, *20*, 153–156. [\[CrossRef\]](#)
47. Peyraube, N.; Lastennet, R.; Denis, A. Geochemical evolution of groundwater in the unsaturated zone of a karstic massif, using the PCO₂–SiC relationship. *J. Hydrol.* **2012**, *430–431*, 13–24. [\[CrossRef\]](#)
48. White, W.B. Carbon fluxes in Karst aquifers: Sources, sinks, and the effect of storm flow. *Acta Carsol.* **2013**, *42*, 177–186. [\[CrossRef\]](#)
49. Probst, J.-L. Géochimie et hydrologie de l'érosion continentale. Mécanismes, bilan global actuel et fluctuations au cours des 500 derniers millions d'années. *Sci. Géol. Mem.* **1992**, *94*, 3–164.
50. Gaillardet, J.; Calmels, D.; Romero-Mujalli, G.; Zakharova, E.; Hartmann, J. Global climate control on carbonate weathering intensity. *Chem. Geol.* **2019**, *527*, 118762. [\[CrossRef\]](#)
51. Reynolds, C.C.; Escobedo, F.J.; Clerici, N.; Zea-Camaño, J. Does “greening” of neotropical cities considerably mitigate carbon dioxide emissions? The case of Medellín, Colombia. *Sustainability* **2017**, *9*, 785. [\[CrossRef\]](#)
52. Rasse, D.P.; François, L.; Aubinet, M.; Kowalski, A.S.; Vande Walle, I.; Laitat, E.; Gérard, J.-C. Modelling short-term CO₂ fluxes and long-term tree growth in temperate forests with ASPECTS. *Ecol. Modell.* **2001**, *141*, 35–52. [\[CrossRef\]](#)
53. Li, S.-L.; Liu, C.-Q.; Li, J.; Lang, Y.-C.; Ding, H.; Li, L. Geochemistry of dissolved inorganic carbon and carbonate weathering in a small typical karstic catchment of Southwest China: Isotopic and chemical constraints. *Chem. Geol.* **2010**, *277*, 301–309. [\[CrossRef\]](#)
54. Ek, C.; Godissart, J. Carbon dioxide in cave air and soil air in some karstic areas of Belgium. A prospective view. *Geol. Belgica* **2014**, *17*, 102–106.
55. Raymond, P.A.; Cole, J.J. Increase in the Export of Alkalinity from North America's Largest River. *Science* **2003**, *301*, 88–91. [\[CrossRef\]](#) [\[PubMed\]](#)
56. Yan, J.; Wang, Y.P.; Zhou, G.; Li, S.; Yu, G.; Li, K. Carbon uptake by karsts in the Houzhai Basin, southwest China. *J. Geophys. Res. Biogeosci.* **2011**, *116*. [\[CrossRef\]](#)
57. Stets, E.G.; Kelly, V.J.; Crawford, C.G. Long-term trends in alkalinity in large rivers of the conterminous US in relation to acidification, agriculture, and hydrologic modification. *Sci. Total Environ.* **2014**, *488–489*, 280–289. [\[CrossRef\]](#)
58. Lespinas, F.; Ludwig, W.; Heussner, S. Impact of recent climate change on the hydrology of coastal Mediterranean rivers in Southern France. *Clim. Chang.* **2010**, *99*, 425–456. [\[CrossRef\]](#)
59. García-Ruiz, J.M.; López-Moreno, J.I.; Vicente-Serrano, S.M.; Lasanta-Martínez, T.; Beguería, S. Mediterranean water resources in a global change scenario. *Earth Sci. Rev.* **2011**, *105*, 121–139. [\[CrossRef\]](#)
60. López-Moreno, J.I.; Vicente-Serrano, S.M.; Moran-Tejeda, E.; Zabalza, J.; Lorenzo-Lacruz, J.; García-Ruiz, J.M. Impact of climate evolution and land use changes on water yield in the Ebro basin. *Hydrol. Earth Syst. Sci.* **2011**, *15*, 311–322. [\[CrossRef\]](#)
61. Brunetti, M.; Buffoni, L.; Mangianti, F.; Maugeri, M.; Nanni, T. Temperature, precipitation and extreme events during the last century in Italy. *Glob. Planet. Chang.* **2004**, *40*, 141–149. [\[CrossRef\]](#)

62. Alpert, P.; Krichak, S.O.; Shafir, H.; Haim, D.; Osetinsky, I. Climatic trends to extremes employing regional modeling and statistical interpretation over the E. Mediterranean. *Glob. Planet. Chang.* **2008**, *63*, 163–170. [\[CrossRef\]](#)
63. Ashofteh, P.S.; Bozorg Haddad, O.; Mariño, M.A. Scenario Assessment of Streamflow Simulation and its Transition Probability in Future Periods Under Climate Change. *Water Resour. Manag.* **2013**, *27*, 255–274. [\[CrossRef\]](#)
64. Rabbinge, R.; Van Diepen, C.A. Changes in agriculture and land use in Europe. *Eur. J. Agron.* **2000**, *13*, 85–99. [\[CrossRef\]](#)
65. García-Ruiz, J.M.; Lana-Renault, N. Hydrological and erosive consequences of farmland abandonment in Europe, with special reference to the Mediterranean region—A review. *Agric. Ecosyst. Environ.* **2011**, *140*, 317–338. [\[CrossRef\]](#)
66. Semhi, K.; Amiotte-Suchet, P.; Clauer, N.; Probst, J.-L. Impact of nitrogen fertilizers on the natural weathering-erosion processes and fluvial transport in the Garonne basin. *Appl. Geochem.* **2000**, *15*, 865–878. [\[CrossRef\]](#)
67. Perrin, A.S.; Probst, A.; Probst, J.-L. Impact of nitrogenous fertilizers on carbonate dissolution in small agricultural catchments: Implications for weathering CO₂ uptake at regional and global scales. *Geochim. Cosmochim. Acta* **2008**, *72*, 3105–3123. [\[CrossRef\]](#)
68. Brunet, F.; Potot, C.; Probst, A.; Probst, J.L. Stable Carbon isotope evidence for nitrogenous fertilizer impact on carbonate weathering in a small agricultural watershed. *Rapid Commun. Mass Spectrom.* **2011**, *25*, 2682–2690. [\[CrossRef\]](#)
69. Probst, A.; Dambrine, E.; Viville, D.; Fritz, B. Influence of acid atmospheric inputs on surface water chemistry and mineral fluxes in a declining spruce stand within a small granitic catchment (Vosges Massif, France). *J. Hydrol.* **1990**, *116*, 101–124. [\[CrossRef\]](#)
70. Li, S.-L.; Calmels, D.; Han, G.; Gaillardet, J.; Liu, C.Q. Sulfuric acid as an agent of carbonate weathering constrained by $\delta^{13}\text{CDIC}$: Examples from Southwest China. *Earth Planet. Sci. Lett.* **2008**, *270*, 189–199. [\[CrossRef\]](#)
71. Ding, H.; Lang, Y.C.; Liu, C.Q.; Liu, T.Z. Chemical characteristics and $\delta^{34}\text{S-SO}_4^{2-}$ of acid rain: Anthropogenic sulfate deposition and its impacts on CO₂ consumption in the rural karst area of southwest China. *Geochem. J.* **2013**, *47*, 625–638. [\[CrossRef\]](#)
72. Probst, A.; Ambroise, B. Disturbance and resilience of a granitic critical zone submitted to acid atmospheric influence (the Ringelbach catchment, Vosges Mountains, France): Lessons from a hydrogeochemical survey in the nineties. *J. Hydrol.* **2019**, *569*, 77–92. [\[CrossRef\]](#)
73. Fonyuy, E.W.; Atekwana, E.A. Effects of acid mine drainage on dissolved inorganic carbon and stable carbon isotopes in receiving streams. *Appl. Geochem.* **2008**, *23*, 743–764. [\[CrossRef\]](#)
74. Ali, H.N.; Atekwana, E.A. The effect of sulfuric acid neutralization on carbonate and stable carbon isotope evolution of shallow groundwater. *Chem. Geol.* **2011**, *284*, 217–228. [\[CrossRef\]](#)
75. Spence, J.; Telmer, K. The role of sulfur in chemical weathering and atmospheric CO₂ fluxes: Evidence from major ions, $\delta^{13}\text{CDIC}$, and $\delta^{34}\text{S SO}_4$ in rivers of the Canadian Cordillera. *Geochim. Cosmochim. Acta* **2005**, *69*, 5441–5458. [\[CrossRef\]](#)
76. Calmels, D.; Gaillardet, J.; Brenot, A.; France-Lanord, C. Sustained sulfide oxidation by physical erosion processes in the Mackenzie River basin: Climatic perspectives. *Geology* **2007**, *35*, 1003–1006. [\[CrossRef\]](#)
77. Lindberg, S.E.; Garten, C.T. Sources of sulphur in forest canopy throughfall. *Nature* **1988**, *336*, 148–151. [\[CrossRef\]](#)
78. Probst, A.; Viville, D.; Fritz, B.; Ambroise, B.; Dambrine, E. Hydrochemical budgets of a small forested granitic catchment exposed to acid deposition: The Strengbach catchment case study (Vosges massif, France). *Water Air Soil Pollut.* **1992**, *62*, 337–347. [\[CrossRef\]](#)
79. Mangin, A. Contribution à L'étude Hydrodynamique des Aquifères Karstiques. Ph.D. Thesis, Université de Dijon, Dijon, France, 1974. (*Ann. Spéléo.*, 1974 29: 283–332; 1974 29: 495–601; 1975 30: 21–124).
80. Labat, D.; Masbou, J.; Beaulieu, E.; Mangin, A. Scaling behavior of the fluctuations in stream flow at the outlet of karstic watersheds, France. *J. Hydrol.* **2011**, *410*, 162–168. [\[CrossRef\]](#)
81. Sivellev, V.; Labat, D.; Mazzilli, N.; Massei, N.; Jourde, H. Dynamics of the Flow Exchanges between Matrix and Conduits in Karstified Watersheds at Multiple Temporal Scales. *Water* **2019**, *11*, 569. [\[CrossRef\]](#)
82. Binet, S.; Probst, J.L.; Batiot, C.; Seidel, J.L.; Emblanch, C.; Peyraube, N.; Charlier, J.B.; Bakalowicz, M.; Probst, A. Global warming and acid atmospheric deposition impacts on carbonate dissolution and CO₂ fluxes in French karst hydrosystems: Evidence from hydrochemical monitoring in recent decades. *Geochim. Cosmochim. Acta* **2020**, *270*, 184–200. [\[CrossRef\]](#)

83. Bakalowicz, M. Contribution de la Géochimie des Eaux à la Connaissance de L'aquifère Karstique et de la Karstification. Ph.D. Thesis, Université Pierre et Marie Curie, Paris, France, 1979.
84. Mangin, A. Le système karstique du Baget (Ariège). *Ann. Spéol.* **1970**, *25*, 560–580.
85. Debrosses, E. Géologie du bassin versant du Baget (zone nord-pyrénéenne, Ariège, France): Nouvelles observations et conséquences. *Assoc. Strata* **2009**, *46*, 1–93.
86. Info Terre: Téléchargement des Cartes Géologiques. Available online: <http://infoterre.brgm.fr/page/telechargement-cartes-geologiques> (accessed on 3 March 2020).
87. Padilla, A.; Pulido-Bosch, A.; Mangin, A. Relative Importance of Baseflow and Quickflow from Hydrographs of Karst Spring. *Groundwater* **1944**, *32*, 267–277. [[CrossRef](#)]
88. Johannet, A.; Vayssade, B.; Bertin, D. Neural Networks: From Black Box towards Transparent Box—Application to Evapotranspiration Modelling. *Int. J. Comput. Intell.* **2008**, *4*, 163–170.
89. Joly, D. Variation spatiale des facteurs qui expliquent le volume des précipitations en France; analyse à échelle locale. In *Journées de Climatologie de la Commission "Climat et Société" du CNFG, Climat et Eau*; Lyon, France, 2011; p. 16. Available online: hal.archives-ouvertes.fr/hal-00941124 (accessed on 23 April 2020).
90. Douguédroit, A.; de Saintignon, M.-F. Les gradients de températures et de précipitations en montagne. *Revue Géograph. Alpine* **1984**, *72*, 225–240.
91. Labat, D.; Ababou, R.; Mangin, A. Rainfall–runoff relations for karstic springs. Part I: Convolution and spectral analyses. *J. Hydrol.* **2000**, *238*, 123–148. [[CrossRef](#)]
92. Jourde, H.; Massei, N.; Mazzilli, N.; Binet, S.; Batiot-Guilhe, C.; Labat, D.; Steinmann, M.; Bailly-Comte, V.; Seidel, J.L.; Arfib, B.; et al. SNO KARST: A french network of observatories for the multidisciplinary study of critical zone processes in karst watersheds and aquifers. *Vadose Zone J.* **2018**, *17*, 1–18. [[CrossRef](#)]
93. Gaillardet, J.; Braud, I.; Hankard, F.; Anquetin, S.; Bour, O.; Dorfliger, N.; de Dreuz, J.R.; Galle, S.; Galy, C.; Gogo, S.; et al. OZCAR: The French network of critical zone observatories. *Vadose Zone J.* **2018**, *17*, 1–24. [[CrossRef](#)]
94. Parr, T.W.; Ferretti, M.; Simpson, I.C.; Forsius, M.; Kovács-Láng, E. Towards A Long-Term Integrated Monitoring Programme In Europe: Network Design in Theory and Practice. *Environ. Monit. Assess* **2002**, *78*, 253–290. [[CrossRef](#)] [[PubMed](#)]
95. Müller, F.; Baessler, C.; Schubert, H.; Klotz, S. (Eds.) *Long-Term Ecological Research. Between Theory and Application*; Springer: Dordrecht, The Netherlands, 2010.
96. ADES—Eau France: Point d'eau BSS002MAYC (10734X0010/HY) BAGET. Available online: <https://ades.eaufrance.fr/Fiche/PtEau?Code=10734X0010/HY> (accessed on 3 March 2020).
97. Clark, I.D.; Fritz, P. *Environmental Isotopes in Hydrogeology*; Lewis Publishers: New York, NY, USA, 1997.
98. Plummer, L.; Busenberg, E. The solubilities of calcite, aragonite and vaterite in CO₂-H₂O solutions between 0 and 90 °C, and an evaluation of the aqueous model for the system CaCO₃-CO₂-H₂O. *Geochim. Cosmochim. Acta* **1982**, *46*, 1011–1040. [[CrossRef](#)]
99. Davies, C.W. The extent of dissociation of salts in water. Part VIII. An equation for the mean ionic activity coefficient of an electrolyte in water, and a revision of the dissociation constants of some sulphates. *J. Chem. Soc.* **1938**, 2093–2098. [[CrossRef](#)]
100. Buishand, T.A. Some methods for testing the homogeneity of rainfall records. *J. Hydrol.* **1982**, *58*, 11–27. [[CrossRef](#)]
101. Buishand, T.A. Tests for detecting a shift in the mean of hydrological time series. *J. Hydrol.* **1984**, *73*, 51–69. [[CrossRef](#)]
102. Piper, A.M. A graphic procedure in geochemical interpretation of water analyses. *Trans. Am. Geophys. Union* **1944**, *25*, 914–923. [[CrossRef](#)]
103. Hamilton. ggtern: An Extension to 'ggplot2', for the Creation of Ternary Diagrams. R Package Version 2.2.2. 2018. Available online: <https://CRAN.R-project.org/package=ggtern> (accessed on 3 March 2020).
104. Petelet, E.; Luck, J.-M.; Ben Othman, D.; Negrel, P.; Aquilina, L. Geochemistry and water dynamics of a medium-sized watershed: The Hérault, southern France: 1. Organisation of the different water reservoirs as constrained by Sr isotopes, major, and trace elements. *Chem. Geol.* **1998**, *150*, 63–83. [[CrossRef](#)]
105. Donnini, M.; Frondini, F.; Probst, J.-L.; Probst, A.; Cardellini, C.; Marchesini, I.; Guzzetti, F. Chemical weathering and consumption of atmospheric carbon dioxide in the Alpine region. *Glob. Planet. Chang.* **2016**, *136*, 65–81. [[CrossRef](#)]

106. El Najjar, P.; Kassouf, A.; Probst, A.; Probst, J.-L.; Ouaini, N.; Daou, C.; El Azzi, D. High-frequency monitoring of surface water quality at the outlet of the Ibrahim River (Lebanon): A multivariate assessment. *Ecol. Indic.* **2019**, *104*, 13–23. [\[CrossRef\]](#)
107. Sarazin, G.; Ciabrini, J.P. Water Geochemistry of Three Mountain Streams from Carbonate Watersheds in the Southern French Alps. *Aquatic Geochem.* **1997**, *3*, 233–265. [\[CrossRef\]](#)
108. Laffitte, P. *Traite D'informatique Géologique*; Masson: Paris, France, 1972; p. 624.
109. Kaiser, H.F. The varimax criterion for analytic rotation in factor analysis. *Psychometrika* **1958**, *23*, 187–200. [\[CrossRef\]](#)
110. Nicholson, R.V.; Gillham, R.W.; Reardon, E.J. Pyrite oxidation in carbonate-buffered solution: 1. Experimental kinetics. *Geochim. Cosmochim. Acta* **1988**, *52*, 1077–1085. [\[CrossRef\]](#)
111. Probst, A.; Lelong, F.; Viville, D.; Durand, P.; Ambroise, B.; Fritz, B. Comparative Hydrochemical Behaviour and Element Budgets of the Aubure (Vosges Massif) and Mont-Lozère (Southern Massif Central) Norway Spruce Forested Catchments. In *Atmospheric Deposition Effects in the French Mountains*; Landmann, G., Bonneau, M., Kaennel, M., Eds.; Springer: Berlin/Heidelberg, Germany, 1995; pp. 203–225.
112. Kayser, N.; Probst, J.-L.; Cadet, D.; Tardy, Y. Propagation des ondes de sécheresse et d'humidité à travers le monde. *Comptes Rendus de l'Académie des Sci. Ser. IIA—Earth Planet.* **1990**, *310*, 757–763.
113. Mangin, A. Transfer function approach for artificial tracer test interpretation in karstic systems. *J. Hydrol.* **2015**, *529*, 866–871.
114. Viers, J.; Oliva, P.; Dandurand, J.; Dupre, B.; Gaillardet, J. Chemical Weathering Rates, CO₂ Consumption, and Control Parameters Deduced from the Chemical Composition of Rivers. In *Treatise on Geochemistry*, 2nd ed.; Holland, H.D., Turekian, K.K., Eds.; Elsevier: Pergamon, NY, USA, 2014; Volume 7, pp. 175–194.
115. Probst, J.-L.; Mortatti, J.; Tardy, Y. Carbon river fluxes and weathering CO₂ consumption in the Congo and Amazon river basins. *Appl. Geochem.* **1994**, *9*, 1–13. [\[CrossRef\]](#)
116. Amiotte-Suchet, P. Cycle du carbone, érosion chimique des continents et transferts vers les océans. *Sci. Géol. Mem.* **1995**, *97*, 3–156.
117. Amiotte-Suchet, P.; Probst, J.-L. Origines du carbone inorganique dissous dans les eaux de la Garonne. Variations saisonnières et interannuelles. *Sci. Géol. Bull.* **1996**, *49*, 101–126.
118. Mortatti, J.; Probst, J.-L. Silicate rock weathering and atmospheric/soil CO₂ uptake in the Amazon basin estimated from river water geochemistry: Seasonal and spatial variations. *Chem. Geol.* **2003**, *197*, 177–196. [\[CrossRef\]](#)
119. Takano, B.; Asano, Y.; Watanuki, K. Characterization of sulfate ion in travertine. *Contrib. Mineral. Petrol.* **1980**, *72*, 197–203. [\[CrossRef\]](#)
120. Stumm, W.; Morgan, J.J. *Aquatic Chemistry—Chemical Equilibria and Rates in Natural Waters*, 3rd ed.; Wiley: New York, NY, USA, 1996.
121. Marcé, R.; Obrador, B.; Morguá, J.A.; Lluís Riera, J.; López, P.; Armengol, J. Carbonate weathering as a driver of CO₂ supersaturation in lakes. *Nat. Geosci.* **2015**, *8*, 107–111. [\[CrossRef\]](#)
122. Ulloa-Cedamano, F. Impacts du Changement Climatique et des Activités Anthropiques sur les Cycles Biogéochimiques du Carbone et de L'azote Dans les Hydrosystèmes Karstiques. Ph.D. Thesis, Toulouse University, Toulouse, France, 2021. (In Progress).
123. Puig, R.; Avila, A.; Soler, A. Sulphur isotopes as tracers of the influence of a coal-fired power plant on a Scots pine forest in Catalonia (NE Spain). *Atmos. Environ.* **2008**, *42*, 733–745. [\[CrossRef\]](#)
124. Pierret, M.C.; Viville, D.; Dambrine, E.; Cotel, S.; Probst, A. Twenty-five-year record of chemicals in open field precipitation and throughfall from a medium-altitude forest catchment (Strengbach—NE France): An obvious response to atmospheric pollution trends. *Atmos. Environ.* **2019**, *202*, 296–314. [\[CrossRef\]](#)
125. Schöpp, W.; Posch, M.; Mylona, S.; Johansson, M. Long-term development of acid deposition (1880–2030) in sensitive freshwater regions in Europe. *Hydrol. Earth Syst. Sci.* **2003**, *7*, 436–446. [\[CrossRef\]](#)
126. Pascaud, A.; Sauvage, S.; Coddeville, P.; Nicolas, M.; Croisé, L.; Mezdoor, A.; Probst, A. Contrasted spatial and long-term trends in precipitation chemistry and deposition fluxes at rural stations in France. *Atmos. Environ.* **2016**, *146*, 28–43. [\[CrossRef\]](#)
127. Pierret, M.C.; Cotel, S.; Ackerer, P.; Beaulieu, E.; Benarioumlil, S.; Boucher, M.; Boutin, R.; Chabaux, F.; Delay, F.; Fourtet, C.; et al. The Strengbach Catchment: A multidisciplinary environmental sentry for 30 years. *Vadose Zone J.* **2018**, *17*, 1–17. [\[CrossRef\]](#)

128. Meybeck, M. Atmospheric Inputs and River Transport of Dissolved Substances. Available online: http://hydrologie.org/redbooks/a141/iahs_141_0173.pdf (accessed on 23 April 2020).
129. Qin, C.; Li, S.; Yue, F.; Xu, S.; Ding, H. Spatiotemporal variations of dissolved inorganic carbon and controlling factors in a small karstic catchment, Southwestern China. *Earth Surf. Process. Landf.* **2019**, *44*, 2423–2436. [[CrossRef](#)]
130. Liu, Z.; Zhao, J. Contribution of carbonate rock weathering to the atmospheric CO₂ sink. *Environ. Geol.* **1999**, *39*, 1053–1058. [[CrossRef](#)]
131. Tipper, E.T.; Bickle, M.J.; Galy, A.; West, A.J.; Pomiès, C.; Chapman, H.J. The short-term climatic sensitivity of carbonate and silicate weathering fluxes: Insight from seasonal variations in river chemistry. *Geochim. Cosmochim. Acta* **2006**, *70*, 2737–2754. [[CrossRef](#)]
132. Probst, J.-L.; Bazerbachi, A. Transports en solution et en suspension par la Garonne supérieure. Solute and particulate transports by the upstream part of the Garonne river. *Sci. Géol. Bull.* **1986**, *39*, 79–98. [[CrossRef](#)]
133. Ladouche, B.; Probst, A.; Viville, D.; Idir, S.; Baqué, D.; Loubet, M.; Probst, J.-L.; Bariac, T. Hydrograph separation using isotopic, chemical and hydrological approaches (Strengbach catchment, France). *J. Hydrol.* **2001**, *242*, 255–274. [[CrossRef](#)]
134. Ponnou-Delaffon, V.; Probst, A.; Payre-Suc, V.; Granouillac, F.; Ferrant, S.; Perrin, A.-S.; Probst, J.-L. Long and short-term trends of stream hydrochemistry and high frequency surveys as indicators of the influence of climate change, agricultural practices and internal processes (Aurade agricultural catchment, SW France). *Ecol. Indic.* **2020**, *110*, 105894. [[CrossRef](#)]
135. Ilstedt, U.; Nordgren, A.; Malmer, A. Optimum soil water for soil respiration before and after amendment with glucose in humid tropical Acrisols and a boreal mor layer. *Soil Biol. Biochem.* **2000**, *32*, 1591–1599. [[CrossRef](#)]
136. Drake, J. The effect of soil activity on the chemistry of carbonate groundwaters. *Water Resour. Res.* **1980**, *16*, 381–386. [[CrossRef](#)]
137. Zhao, Q.; Chang, D.; Wang, K.; Huang, J. Patterns of nitrogen export from a seasonal freezing agricultural watershed during the thawing period. *Sci. Total Environ.* **2017**, *599–600*, 442–450. [[CrossRef](#)]
138. Van Rempelbergh, M.; Verheyden, S.; Allan, M.; Quinif, Y.; Keppens, E.; Claeys, P. Monitoring of a fast-growing speleothem site from the Han-sur-Lesse cave, Belgium, indicates equilibrium deposition of the seasonal $\delta^{18}\text{O}$ and $\delta^{13}\text{C}$ signals in the calcite. *Clim. Past* **2014**, *10*, 1871–1885. [[CrossRef](#)]
139. Telmer, K.; Veizer, J. Carbon fluxes, pCO₂ and substrate weathering in a large northern river basin, Canada: Carbon isotope perspectives. *Chem. Geol.* **1999**, *159*, 61–86. [[CrossRef](#)]
140. Klimchouk, A.-B. Towards defining, delimiting and classifying epikarst: Its origin, processes and variants of geomorphic evolution. *Speleogenesis Evol. Karst Aquifers* **2004**, *2*, 1–13.
141. Zou, S.; Deng, Z.; Zhu, Y.; Liang, B.; Xia, R.; Tang, J. Hydrologic Features and Eco-Environmental Classification of Epikarst Springs in Luota, West of Hunan, China. *Earth Sci. Front.* **2008**, *15*, 190–197. [[CrossRef](#)]
142. Aquilina, L.; Ladouche, B.; Dörfli, N. Water storage and transfer in the epikarst of karstic systems during high flow periods. *J. Hydrol.* **2006**, *327*, 472–485. [[CrossRef](#)]
143. Trček, B. How can the epikarst zone influence the karst aquifer hydraulic behaviour? *Environ. Geol.* **2007**, *51*, 761–765. [[CrossRef](#)]
144. Peyraube, N.; Lastennet, R.; Denis, A.; Malaurent, P. Estimation of epikarst air PCO₂ using measurements of water $\delta^{13}\text{C}$ TDIC, cave air PCO₂ and $\delta^{13}\text{C}$ CO₂. *Geochim. Cosmochim. Acta* **2013**, *118*, 1–17. [[CrossRef](#)]
145. Walling, D.E.; Foster, I.D.L. Variations in the natural chemical concentration of river water during flood flows, and the lag effect: Some further comments. *J. Hydrol.* **1975**, *26*, 237–244. [[CrossRef](#)]
146. Mahamat Nour, A.; Vallet-Coulomb, C.; Bouchez, C.; Ginot, P.; Doumnang, J.C.; Sylvestre, F.; Deschamps, P. Geochemistry of the Lake Chad Tributaries Under Strongly Varying Hydro-climatic Conditions. *Aquat. Geochem.* **2020**, *26*, 3–29. [[CrossRef](#)]
147. Kämäri, M.; Tattari, S.; Lotsari, E.; Koskiahio, J.; Lloyd, C.-E.-M. High-frequency monitoring reveals seasonal and event-scale water quality variation in a temporally frozen river. *J. Hydrol.* **2018**, *564*, 619–639. [[CrossRef](#)]
148. Martínez-Santos, M.; Antigüedad, I.; Ruiz-Romera, E. Hydrochemical variability during flood events within a small forested catchment in Basque Country (Northern Spain). *Hydrol. Process.* **2014**, *28*, 5367–5381. [[CrossRef](#)]

149. Bovolín, V.; Cuomo, A.; Guida, D. Monitoring activity at the Middle Bussento Karst System (Cilento Geopark, southern Italy). *Eng. Geol. Soc. Territ.* **2015**, *3*, 275–279.
150. Qin, C.; Li, S.-L.; Waldron, S.; Yue, F.-J.; Wang, Z.-J.; Zhong, J.; Ding, H.; Liu, C.-Q. High-frequency monitoring reveals how hydrochemistry and dissolved carbon respond to rainstorms at a karstic critical zone, Southwestern China. *Sci. Total Environ.* **2020**, *714*, 136833. [[CrossRef](#)]



© 2020 by the authors. Licensee MDPI, Basel, Switzerland. This article is an open access article distributed under the terms and conditions of the Creative Commons Attribution (CC BY) license (<http://creativecommons.org/licenses/by/4.0/>).